PHYSICAL REVIEW D **85,** 074501 (2012)

Lattice study on πK scattering with moving wall source

Ziwen Fu

Key Laboratory of Radiation Physics and Technology (Sichuan University), Ministry of Education; Institute of Nuclear Science and Technology, Sichuan University, Chengdu 610064, People's Republic of China

(Received 19 September 2011; revised manuscript received 3 February 2012; published 2 April 2012)

The s-wave pion-kaon (πK) scattering lengths at zero momentum are calculated in lattice QCD with sufficiently light u/d quarks and strange quark at its physical value by the finite size formula. The light quark masses correspond to $m_\pi = 0.330$–0.466 GeV. In the Asqtad improved staggered fermion formulation, we measure the πK four-point correlators for both the isospin $I = 1/2$ and $3/2$ channels, and analyze the lattice simulation data at the next-to-leading order in the continuum three-flavor chiral perturbation theory, which enables a simultaneous extrapolation of πK scattering lengths at the physical point. We adopt a technique with the moving wall sources without gauge fixing to obtain substantiable accuracy; moreover, for the $I = 1/2$ channel, we employ the variational method to isolate the contamination from the excited states. Extrapolating to the physical point yields the scattering lengths as $m_\pi a_{3/2} = -0.0512(18)$ and $m_\pi a_{1/2} = 0.1819(35)$ for the $I = 3/2$ and $1/2$ channels, respectively. Our simulation results for πK scattering lengths are in agreement with the experimental reports and theoretical predictions, and can be comparable with other lattice simulations. These simulations are carried out with MILC $N_f = 2 + 1$ flavor gauge configurations at lattice spacing $a \approx 0.15$ fm.

DOI: 10.1103/PhysRevD.85.074501 PACS numbers: 12.38.Gc

I. INTRODUCTION

Pion-kaon (πK) scattering at low energies is the simplest reaction including a strange quark, and it allows for an explicit exploration of the three-flavor structure of the low-energy hadronic interactions, which is not directly probed in the $\pi\pi$ scattering. The measurement of πK scattering lengths is one of the cleanest processes and a decisive test for our understanding of the chiral SU(3) symmetry breaking of the quantum chromodynamics (QCD). In the present study, we will concentrate on the s-wave scattering lengths of the πK system, which have two isospin eigenchannels ($I = 3/2$, $1/2$) in the isospin limit, and the low-energy interaction is repulsive for the $I = 3/2$ channel, and attractive for the $I = 1/2$ case, respectively.

Experimentally, πK scattering lengths are obtained through πK scattering phases using the Roy-Steiner equations. The experiments at low energies are an important method in the study of the interactions among mesons [1–3], and these experiments have reported that the s-wave scattering length (a_0) in the $I = 3/2$ channel, $m_\pi a_{3/2}$, has a small negative value, namely, -0.13– -0.05. Moreover, the ongoing experiments proposed by the DIRAC Collaboration [4] to examine πK atoms will provide the direct measurements or constraints on πK scattering lengths.

At present, theory predicts πK scattering lengths with a precision of about 10%, and it will be significantly improved in the near future. Through the scalar form factors in semileptonic pseudoscalar-to-pseudoscalar decays, Flynn and Nieves [5] extracted the πK scattering length in the $I = 1/2$ channel as $m_\pi a_{1/2} = +0.179(17)(14)$. Three-flavor chiral perturbation theory (χPT) [6–9] has been used to predict the scattering lengths in the study of the low-energy πK scattering, and a small negative value was claimed as $m_\pi a_{3/2} = -0.129$– -0.05. However, if the scattering hadrons contain strange quarks, χPT predictions usually suffer from considerable corrections due to the chiral SU(3) flavor symmetry breaking, as compared with the case of the $\pi\pi$ scattering. Therefore, a lattice QCD calculation is needed to offer an alternative important, consistent check of the validity of χPT in the presence of the strange quarks.

To date, four lattice studies of πK scattering length have been reported [10–13]. The first lattice calculation of πK scattering length in the $I = 3/2$ channel was explored by Miao *et al.* [10] using the quenched approximation, and the value of $m_\pi a_{3/2}$ was found to be -0.048. The first fully dynamical calculation using $N_f = 2 + 1$ flavors of the Asqtad-improved [14,15] staggered sea quark [16,17] was carried out in [11] to calculate the $I = 3/2$ scattering length for $m_\pi = 0.29$–0.60 GeV, and further indirectly evaluate the $I = 1/2$ scattering length on the basis of χPT. Beane *et al.* [11] obtained a small negative value of $m_\pi a_{3/2} = -0.0574$ for the $I = 3/2$ channel and a positive value of $m_\pi a_{1/2} = 0.1725$ for the $I = 1/2$ channel, respectively. Nagata *et al.* fulfilled the first direct lattice calculation on the $I = 1/2$ channel [12] using the quenched approximation. They investigated all quark diagrams contributing to both isospin eigenstates, and found that the scattering amplitudes can be expressed as the combinations of only three diagrams in the isospin limit. This work greatly inspired us to study πK scattering. However, they did not observe the repulsive interaction even for the $I = 3/2$ channel at their simulation points, and

their lattice calculations are relatively cheaper. Sasaki *et al.* observed the correct repulsive interaction for the $I = 3/2$ channel and attractive for the $I = 1/2$ case, and they obtained the scattering lengths of $m_\pi a_{3/2} = -0.0500(68)$ and $m_\pi a_{1/2} = 0.154(28)$ for the $I = 3/2$ and $1/2$ channels, respectively [13]. Moreover, to isolate the contamination from the excited states, they constructed a 2×2 matrix of the time correlation function and diagonalized it [13]; this method will guide us to study πK scattering for the $I = 1/2$ channel in a correct manner. It should be stressed that, to reduce the computational cost, they employed a technique with a ''fixed'' kaon sink operator for the calculation of πK scattering length in the $I = 1/2$ channel and then an exponential factor was introduced to drop the unnecessary t dependence appearing due to the fixed kaon sink time [13]. In this work, we will improve this technique by using a ''moving'' wall source without gauge fixing where the exponential factor is not needed any more.[1] Thus, there has been no satisfactory direct lattice calculation for the $I = 1/2$ channel until now.

In the present study, we will use the MILC gauge configurations generated in the presence of $N_f = 2 + 1$ flavors of the Asqtad-improved [14,15] staggered dynamical sea quarks [16,17] to study the s-wave πK scattering lengths for both the $I = 1/2$ and $3/2$ channels. Inspired by the exploratory studies of the $\pi\pi$ scattering for the $I = 0$ channel in Refs. [18,19], we will adopt the same technique, and use the moving kaon wall source operator without gauge fixing for the $I = 1/2$ and $3/2$ channels to obtain the reliable accuracy. We calculated all the three diagrams categorized in Ref. [12], and observed a clear signal of attraction for the $I = 1/2$ channel and that of repulsion for the $I = 3/2$ case. Moreover, for the $I = 1/2$ channel, we employed the variational method to isolate the contamination from the excited states. Most of all, we only used the lattice simulation data of our measured πK scattering lengths for both isospin eigenstates to simultaneously extrapolate toward the physical point using the continuum three-flavor χPT at the next-to-leading order. Our lattice simulation results of the scattering lengths for both isospin eigenchannels are in accordance with the experimental reports and theoretical predictions, and are comparable with other lattice simulations.

This article is organized as follows. In Sec. II we will describe the formalism for the calculation of πK scattering lengths including the Lüscher's formula [20–22] and our computational technique of the modified wall sources for the measurement of πK four-point functions. In Sec. III we will show the simulation parameters and our concrete lattice calculations. We will present our lattice simulation results in Sec. IV, and arrive at our conclusions and outlooks in Sec. V. Some details of the numerical calculation are provided in the appendixes for reference.

[1] In fact, we use the same technique in Refs. [18,19] for $\pi\pi$ scattering. We call it a moving wall source, and just want to emphasize that it is distinguished from the one with a fixed wall in Ref. [13].

II. METHOD OF MEASUREMENT

In this section, we will briefly review the formulas of the s-wave scattering length from two-particle energy in a finite box, with emphasis on the formulas for the isospin $I = 1/2$ πK system. Also we will present the detailed procedure for extracting the energies of the πK system. Here we follow the original derivations and notations in Refs. [12,18,19,23,24].

A. πK four-point functions

Let us consider the πK scattering of one Nambu-Goldstone pion and one Nambu-Goldstone kaon in the Asqtad-improved staggered dynamical fermion formalism. Using operators $O_\pi(x_1)$, $O_\pi(x_3)$ for pions at points x_1, x_3, and operators $O_K(x_2)$, $O_K(x_4)$ for kaons at points x_2, x_4, respectively, with the pion and kaon interpolating field operators defined by

$$\begin{aligned}
\mathcal{O}_{\pi^+}(\mathbf{x}, t) &= -\bar{d}(\mathbf{x}, t)\gamma_5 u(\mathbf{x}, t), \\
\mathcal{O}_{\pi^0}(\mathbf{x}, t) &= \frac{1}{\sqrt{2}}[\bar{u}(\mathbf{x}, t)\gamma_5 u(\mathbf{x}, t) - \bar{d}(\mathbf{x}, t)\gamma_5 d(\mathbf{x}, t)], \\
\mathcal{O}_{K^0}(\mathbf{x}, t) &= \bar{s}(\mathbf{x}, t)\gamma_5 d(\mathbf{x}, t), \\
\mathcal{O}_{K^+}(\mathbf{x}, t) &= \bar{s}(\mathbf{x}, t)\gamma_5 u(\mathbf{x}, t),
\end{aligned} \tag{1}$$

we then represent the πK four-point functions as

$$C_{\pi K}(x_4, x_3, x_2, x_1) = \langle \mathcal{O}_K(x_4)\mathcal{O}_\pi(x_3)\mathcal{O}_K^\dagger(x_2)\mathcal{O}_\pi^\dagger(x_1)\rangle, \tag{2}$$

where $\langle \cdots \rangle$ represents the expectation value of the path integral, which we evaluate using the lattice QCD simulations.

After summing over spatial coordinates $\mathbf{x}_1$, $\mathbf{x}_2$, $\mathbf{x}_3$, and $\mathbf{x}_4$, we obtain the πK four-point function in the zero-momentum state,

$$C_{\pi K}(t_4, t_3, t_2, t_1) = \sum_{\mathbf{x}_1}\sum_{\mathbf{x}_2}\sum_{\mathbf{x}_3}\sum_{\mathbf{x}_4} C_{\pi K}(x_4, x_3, x_2, x_1), \tag{3}$$

where $x_1 \equiv (\mathbf{x}_1, t_1)$, $x_2 \equiv (\mathbf{x}_2, t_2)$, $x_3 \equiv (\mathbf{x}_3, t_3)$, and $x_4 \equiv (\mathbf{x}_4, t_4)$, and t stands for the time difference, namely, $t \equiv t_3 - t_1$.

To avoid the complicated Fierz rearrangement of the quark lines, we choose the creation operators at the time slices which are different by one lattice time spacing as is suggested in Ref. [19], namely, we select $t_1 = 0$, $t_2 = 1$, $t_3 = t$, and $t_4 = t + 1$. In the πK system, there are two isospin eigenstates, namely, $I = 3/2$ and $I = 1/2$; we construct the πK operators for these isospin eigenchannels as [12]

$$\mathcal{O}_{\pi K}^{I=(1/2)}(t) = \frac{1}{\sqrt{3}}\{\sqrt{2}\pi^+(t)K^0(t+1) - \pi^0(t)K^+(t+1)\},$$
$$\mathcal{O}_{\pi K}^{I=(3/2)}(t) = \pi^+(t)K^+(t+1), \tag{4}$$

where

$$\mathcal{O}_{K^0}(t) = \sum_{\mathbf{x}} \mathcal{O}_{K^0}(\mathbf{x}, t), \qquad \mathcal{O}_{K^+}(t) = \sum_{\mathbf{x}} \mathcal{O}_{K^+}(\mathbf{x}, t),$$
$$\mathcal{O}_{\pi^0}(t) = \sum_{\mathbf{x}} \mathcal{O}_{\pi^0}(\mathbf{x}, t), \qquad \mathcal{O}_{\pi^+}(t) = \sum_{\mathbf{x}} \mathcal{O}_{\pi^+}(\mathbf{x}, t). \tag{5}$$

If we assume that the u and d quarks have the same mass, only three diagrams contribute to πK scattering amplitudes [12]. The quark line diagrams contributing to the πK four-point function denoted in Eq. (3) are displayed in Fig. 1, and labeled as direct (D), crossed (C), and rectangular (R), respectively. The direct and crossed diagrams can be easily evaluated by constructing the corresponding four-point amplitudes for arbitrary values of the time slices t_3 and t_4 using only two wall sources placed at the fixed time slices t_1 and t_2. However, the rectangular diagram (R) requires another quark propagator connecting the time slices t_3 and t_4, which make the reliable evaluation of this diagram extremely difficult.

Sasaki *et al.*. solve this problem through the technique with a fixed kaon sink operator to reduce the computational cost [13]. Encouraged by the exploratory works of the $\pi\pi$ scattering at the $I = 0$ channel in Refs. [18,19], in the same way, we handle this problem by evaluating T quark propagators on a $L^3 \times T$ lattice: each propagator, which corresponds to a wall source at the time slice $t = 0, \cdots, T-1$, is denoted by

$$\sum_{n''} D_{n',n''} G_t(n'') = \sum_{\mathbf{x}} \delta_{n',(\mathbf{x},t)}, \qquad 0 \le t \le T-1, \tag{6}$$

where D is the quark matrix for the staggered Kogut-Susskind quark action. The combination of $G_t(n)$ which we apply for πK four-point functions is schematically shown in Fig. 1, where short bars stand for the position of the wall source, open circles are sinks for local pion or kaon operators, and the thicker lines represent the strange quark lines. Likely, the subscript t in the quark propagator

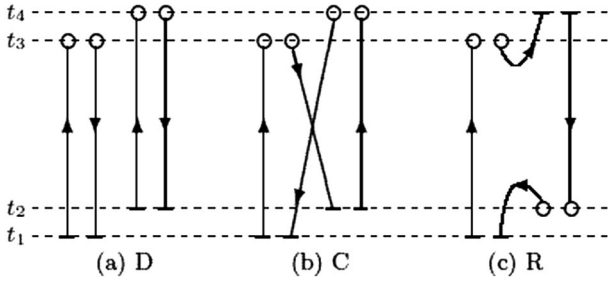

FIG. 1. Diagrams contributing to πK four-point functions. Short bars stand for wall sources. Open circles are sinks for local pion or kaon operators. The thicker lines represent the strange quark lines.

G represents the position of the wall source. D, C, and R, are schematically displayed in Fig. 1, and we can also expressed them in terms of the quark propagators G, namely,

$$\begin{aligned} C^D(t_4,t_3,t_2,t_1) &= \sum_{\mathbf{x}_3}\sum_{\mathbf{x}_4}\langle \mathrm{Re\,Tr}[G^\dagger_{t_1}(\mathbf{x}_3,t_3)G_{t_1}(\mathbf{x}_3,t_3) \\ &\quad \times G^\dagger_{t_2}(\mathbf{x}_4,t_4)G_{t_2}(\mathbf{x}_4,t_4)]\rangle, \\ C^C(t_4,t_3,t_2,t_1) &= \sum_{\mathbf{x}_3}\sum_{\mathbf{x}_4}\langle \mathrm{Re\,Tr}[G^\dagger_{t_1}(\mathbf{x}_3,t_3)G_{t_2}(\mathbf{x}_3,t_3) \\ &\quad \times G^\dagger_{t_2}(\mathbf{x}_4,t_4)G_{t_1}(\mathbf{x}_4,t_4)]\rangle, \\ C^R(t_4,t_3,t_2,t_1) &= \sum_{\mathbf{x}_2}\sum_{\mathbf{x}_3}\langle \mathrm{Re\,Tr}[G^\dagger_{t_1}(\mathbf{x}_2,t_2)G_{t_4}(\mathbf{x}_2,t_2) \\ &\quad \times G^\dagger_{t_4}(\mathbf{x}_3,t_3)G_{t_1}(\mathbf{x}_3,t_3)]\rangle, \end{aligned} \tag{7}$$

where daggers mean the conjugation by the even-odd parity $(-1)^n$ for the staggered Kogut-Susskind quark action, and Tr stands for the trace over the color index. The Hermiticity properties of the propagator G are used to eliminate the factors of γ^5.

The πK rectangular diagram in Fig. 1(c) creates the gauge-variant noise [18,19]. One can reduce the noise by fixing gauge configurations to some gauge (e.g., the Coulomb gauge), and select a special wall source to emit only the Nambu-Goldstone pion [25]; however, the gauge noninvariant states may contaminate the πK four-point function. Alternatively, we perform the gauge field average without gauge fixing since the gauge dependent fluctuations should neatly cancel out among the lattice configurations. Besides these cancellations, the summation of the gauge-variant terms over the spatial sites of the wall source further suppresses the gauge-variant noise. In our current lattice simulation we found that this method works pretty well.

All three diagrams in Fig. 1 need to be calculated to study the πK scattering in both the $I = 1/2$ and $3/2$ channels. Three types of the propagators can be combined to construct the physical correlation functions for πK states with definite isospin. As investigated in Ref. [12], in the isospin limit, the πK correlation function for the $I = 3/2$ and $1/2$ channels can be expressed as the combinations of three diagrams, namely,

$$\begin{aligned} C_{\pi K}^{I=(1/2)}(t) &\equiv \langle \mathcal{O}_{\pi K}^{I=(1/2)}(t) | \mathcal{O}_{\pi K}^{I=(1/2)}(0)\rangle \\ &= D + \tfrac{1}{2}N_f C - \tfrac{3}{2}N_f R, \\ C_{\pi K}^{I=(3/2)}(t) &\equiv \langle \mathcal{O}_{\pi K}^{I=(3/2)}(t) | \mathcal{O}_{\pi K}^{I=(3/2)}(0)\rangle = D - N_f C, \end{aligned} \tag{8}$$

where the operator $\mathcal{O}^I_{\pi K}$ denoted in Eq. (4) creates a πK state with total isospin I and the staggered-flavor factor N_f is inserted to correct for the flavor degrees of freedom of the Kogut-Susskind staggered fermion [24]. For pion and kaon operators it is most natural to choose the ones in the Nambu-Goldstone channel. This is our choice.

To calculate the scattering lengths for hadron-hadron scattering on the lattice, or the scattering phase shifts in general, one usually resorts to Lüscher's formula which relates the exact energy level of two hadron states in a finite box to the scattering phase shift in the continuum. In the case of πK scattering, the s-wave πK scattering length in the continuum is defined by

$$a_0 = \lim_{k\to 0} \frac{\tan\delta_0(k)}{k}. \tag{9}$$

k is the magnitude of the center-of-mass scattering momentum which is related to the total energy $E^I_{\pi K}$ of the πK system with isospin I in a finite box of size L by

$$E^I_{\pi K} = \sqrt{m_\pi^2 + k^2} + \sqrt{m_K^2 + k^2}, \tag{10}$$

where m_π is pion mass, and m_K is kaon mass. We can rewrite Eq. (10) to an elegant form as

$$k^2 = \frac{1}{4}\left(E^I_{\pi K} + \frac{m_\pi^2 - m_K^2}{E^I_{\pi K}}\right)^2 - m_\pi^2. \tag{11}$$

In the absence of the interactions between the π and K particles, $k/\tan\delta_0(k) \to \infty$, and the energy levels occur at momenta $k = 2\pi n/L$ (n is a integer), corresponding to the single-particle modes in a cubic box. $\delta_0(k)$ is the s-wave scattering phase shift, which can be evaluated by the Lüscher's finite size formula [20,22],

$$\left(\frac{\tan\delta_0(k)}{k}\right)^{-1} = \frac{\sqrt{4\pi}}{\pi L}\cdot \mathcal{Z}_{00}\left(1, \frac{k^2}{(2\pi/L)^2}\right), \tag{12}$$

where the zeta function $\mathcal{Z}_{00}(1; q^2)$ is denoted by

$$\mathcal{Z}_{00}(1; q^2) = \frac{1}{\sqrt{4\pi}} \sum_{\mathbf{n}\in\mathbb{Z}^3} \frac{1}{n^2 - q^2}; \tag{13}$$

here $q = kL/(2\pi)$ is no longer an integer, and $\mathcal{Z}_{00}(1; q^2)$ can be efficiently calculated by the method described in Ref. [26]. We also discuss this technique in Appendix A, where we extend this discussion to the case with the negative q^2. In the case of the attractive interaction, k^2 on the bound state has a negative value; therefore k is purely imaginary, and $\delta_0(k)$ is no longer a physical scattering phase shift [13]. $\mathcal{Z}_{00}(1, q^2)$, however, still have a real value even for this case; hence $\tan\delta_0(k)/k$ obtained by Eq. (12) is also real. If $|k^2|$ is small enough, we can consider $\tan\delta_0(k)/k$ as the physical scattering length at the πk threshold [13].

The energy $E^I_{\pi K}$ of the πK system with isospin I can be obtained from the πK four-point function denoted in Eq. (8) with the large t. At large t these correlators will behave as [27,28]

$$C^I_{\pi K}(t) = Z_{\pi K}\cosh\left[E^I_{\pi K}\left(t - \frac{T}{2}\right)\right] + (-1)^t Z'_{\pi K}\cosh\left[E^{I\prime}_{\pi K}\left(t - \frac{T}{2}\right)\right] + \cdots, \tag{14}$$

where $E^I_{\pi K}$ is the energy of the lightest πK state with isospin I. The terms alternating in sign are a peculiarity of the Kogut-Susskind formulation of the lattice fermions and correspond to the contributions from intermediate states with opposite parity [27,28]. The ellipsis suggests the contributions from excited states which are suppressed exponentially.

We should bear in mind that, for the staggered Kogut-Susskind quark action, there are further complications in themselves stemming from the nondegeneracy of pions and kaons in the Goldstone and other channels at a finite lattice spacing. Briefly speaking, the contributions of non-Nambu-Goldstone pions and kaons in the intermediate states is exponentially suppressed for long periods of time due to their heavier masses compared to those of the Nambu-Goldstone pion and kaon [18,19,24]. Thus, we suppose that the πK interpolator does not couple significantly to other πK tastes, and neglect these systematic errors.

In our concrete calculation, we calculated the pion mass m_π and kaon mass m_K through the methods discussed by the MILC Collaboration in Refs. [29,30] in our previous study [31]. In this work we evaluate the total energy $E^I_{\pi K}$ of the πK system with isospin I from Eq. (14).

In the current study we also evaluate the energy shift $\delta E_I = E^I_{\pi K} - (m_\pi + m_K)$ from the ratios

$$R^X(t) = \frac{C^X_{\pi K}(0, 1, t, t+1)}{C_\pi(0, t) C_K(1, t+1)}, \qquad X = D, C, \quad \text{and} \quad R, \tag{15}$$

where $C_\pi(0, t)$ and $C_K(1, t+1)$ are the pion and kaon two-point functions, respectively. Considering Eq. (8), we can write the amplitudes which project out the $I = 1/2$ and $3/2$ isospin eigenstates as

$$\begin{aligned} R_{I=(1/2)}(t) &= R^D(t) + \tfrac{1}{2}N_f R^C(t) - \tfrac{3}{2}N_f R^R(t), \\ R_{I=(3/2)}(t) &= R^D(t) - N_f R^C(t). \end{aligned} \tag{16}$$

Following the discussions in Ref. [24], we now can extract the energy shift δE_I from the ratios

$$R_I(t) = Z_I e^{-\delta E_I t} + \cdots, \tag{17}$$

where Z_I stands for the wave function factor, which is the ratio of two amplitudes from the πK four-point function and the square of the pion two-point correlator and the kaon two-point correlator, and the ellipsis indicates the terms suppressed exponentially. In $R_I(t)$, some of the fluctuations which contribute to both the two-point and four-point correlation functions neatly cancel out, hence, improving the quality of the extraction of the energy shift as compared with what we can obtain from an analysis through the individual correlation functions [11].

For the $I = 3/2$ channel, we can use Eq. (14) or Eq. (17) to extract the energy shifts δE. We have numerically compared the fitting values from two methods, and found

good agreement within statistical errors. In fact, using Eq. (17) to extract the energy shift δE has been extensively employed for the study of πK scattering at the $I = 3/2$ case in Ref. [11]. Hence, in this work, we will only present the energy shifts δE calculated by Eq. (17), and then their corresponding scattering lengths.

On the other hand, for the $I = 1/2$ channel, the presence of the kappa resonance is clearly shown in the low energy [13], and therefore it should be necessary for us to separate the ground state contribution from the contamination stemming from the excited states to achieve the reliable scattering length as investigated in Ref. [13]. For this purpose, we will construct a 2×2 correlation matrix of the time correlation function and diagonalize it to extract the energy of the ground state.

B. Correlation matrix

For the $I = 1/2$ channel, to separate the contamination from the excited states, we construct a matrix of the time correlation function,

$$C(t) = \begin{pmatrix} \langle 0|\mathcal{O}^{\dagger}_{\pi K}(t)\mathcal{O}_{\pi K}(0)|0\rangle & \langle 0|\mathcal{O}^{\dagger}_{\pi K}(t)\mathcal{O}_{\kappa}(0)|0\rangle \\ \langle 0|\mathcal{O}^{\dagger}_{\kappa}(t)\mathcal{O}_{\pi K}(0)|0\rangle & \langle 0|\mathcal{O}^{\dagger}_{\kappa}(t)\mathcal{O}_{\kappa}(0)|0\rangle \end{pmatrix}, \tag{18}$$

where $\mathcal{O}_{\kappa}(t)$ is an interpolating operator for the κ meson with zero momentum, and $\mathcal{O}_{\pi K}(t)$ is an interpolating operator for the πK system which is extensively discussed in Sec. II A. The interpolating operator $\mathcal{O}_{\kappa}$ employed here is exactly the same as those in our previous studies in Refs. [31–33], and the notations adopted here are also the same, but to make this paper self-contained, all the necessary definitions will be also presented below.

1. κ sector

In our previous studies [31–33], we have presented a detailed procedure to measure the kappa correlator $\langle 0|\kappa^{\dagger}(t)\kappa(0)|0\rangle$. To simulate the correct number of quark species, we use the fourth-root trick [34], which automatically performs the transition from four tastes to one taste per flavor for the staggered fermion at all orders. We employ an interpolation operator with isospin $I = 1/2$ and $J^P = 0^+$ at the source and sink,

$$\mathcal{O}(x) \equiv \frac{1}{\sqrt{n_r}} \sum_{a,g} \bar{s}^a_g(x) u^a_g(x), \tag{19}$$

where g is the indices of the taste replica, n_r is the number of the taste replicas, a is the color indices, and we omit the Dirac-Spinor index. The time slice correlator for the κ meson in the zero-momentum state can be evaluated by

$$C_{\kappa}(t) = \frac{1}{n_r} \sum_{\mathbf{x},a,b} \sum_{g,g'} \langle \bar{s}^b_{g'}(\mathbf{x}, t) u^b_{g'}(\mathbf{x}, t) \bar{u}^a_g(\mathbf{0}, 0) s^a_g(\mathbf{0}, 0)\rangle,$$

where $\mathbf{0}$, $\mathbf{x}$ are the spatial points of the κ state at source and sink, respectively. After performing Wick contractions of fermion fields, and summing over the taste index, for the light u quark Dirac operator M_u and the s quark Dirac operator M_s, we obtain [31]

$$C_{\kappa}(t) = \sum_{\mathbf{x}} (-)^x \langle \mathrm{Tr}[M_u^{-1}(\mathbf{x}, t; 0, 0) M_s^{-1^{\dagger}}(\mathbf{x}, t; 0, 0)]\rangle, \tag{20}$$

where Tr is the trace over the color index, and $x = (\mathbf{x}, t)$ is the lattice position.

For the staggered quarks, the meson propagators have the generic single-particle form,

$$\mathcal{C}(t) = \sum_i A_i e^{-m_i t} + \sum_i A'_i (-1)^t e^{-m'_i t} + (t \rightarrow N_t - t), \tag{21}$$

where the oscillating terms correspond to a particle with opposite parity. For the κ meson correlator, we consider only one mass with each parity in Eq. (21); namely, in our concrete calculation, our operator is the state with spin-taste assignment $I \otimes I$ and its oscillating term with $\gamma_0\gamma_5 \otimes \gamma_0\gamma_5$ [31]. Thus, the κ correlator was fit to the following physical model:

$$C_{\kappa}(t) = b_{\kappa} e^{-m_{\kappa} t} + b_{K_A} (-)^t e^{-M_{K_A} t} + (t \rightarrow N_t - t), \tag{22}$$

where b_{K_A} and b_{κ} are two overlap factors. In Fig. 6, we clearly note this oscillating term.

We should bear in mind that, for the staggered Kogut-Susskind quark action, our κ interpolating operator couples to various tastes as we examined the scalar a_0 and σ mesons in Refs. [35–39], where we investigated two-pseudoscalar intermediates states (namely, bubble contribution). In Ref. [32], we investigated the extracted κ masses with and without bubble contribution for kappa correlators. We found that there exist about 2%–5% differences in kappa masses, and the bubble contributions are dominant in the κ correlators at a large time region. Therefore, in the current study, we will investigate whether the bubble contribution has a large influence on the final result of the scattering length or not.

2. Off-diagonal sector

The calculations of the off-diagonal elements in correlation matrix $C(t)$ in Eq. (18), namely, $\langle 0|\mathcal{O}^{\dagger}_{\pi K}(t)\mathcal{O}_{\kappa}(0)|0\rangle$ and $\langle 0|\mathcal{O}^{\dagger}_{\kappa}(t)\mathcal{O}_{\pi K}(0)$, are exactly the same as those in our previous study for nonzero momenta in Ref. [33]; the notations adopted here are also the same, but to make this paper self-contained, all the necessary definitions will also be presented below.

To avoid the complicated Fierz rearrangement of the quark lines, we choose the creation operators at the time slices which are different by one lattice time spacing as suggested in Ref. [19]; namely, we select $t_1 = 0$, $t_2 = 1$, and $t_3 = t$ for the $\pi K \rightarrow \kappa$ three-point function, and choose $t_1 = 0$, $t_2 = t$, and $t_3 = t + 1$ for the $\kappa \rightarrow \pi K$ three-point function.

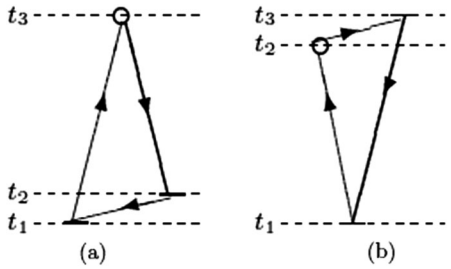

FIG. 2. Diagrams contributing to $\pi K \to \kappa$ and $\kappa \to \pi K$ three-point functions. Short bars stand for wall sources. The thicker lines represent the strange quark lines. (a) Quark contractions of $\pi K \to \kappa$, where open circle is sink for local kappa operator. (b) Quark contractions of $\kappa \to \pi K$, where open circle is sink for local pion operator.

The quark line diagrams contributing to $\pi K \to \kappa$ and $\kappa \to \pi K$ three-point functions are plotted in Fig. 2(a) and Fig. 2(b), respectively, where short bars stand for the position of wall source, open circles are sinks for local pion or kaon operators, and the thicker lines represent the strange quark lines. Likely, the subscript t in the quark propagator G represents the position of the corresponding wall source.

The $\pi K \to \kappa$ three-point function can be easily evaluated by constructing the corresponding three-point amplitudes for arbitrary values of the time slice t_3 using only two wall sources placed at the fixed time slices t_1 and t_2. However, the calculation of the $\kappa \to \pi K$ three-point function is almost equally difficult to that of the rectangular diagram for the πK four-point correlator function, since it requires another quark propagator connecting time slices t_2 and t_3. The $\kappa \to \pi K$ and $\pi K \to \kappa$ three-point functions are schematically shown in Fig. 2, and we can also express them in terms of the quark propagators G, namely,

$$\begin{aligned} C_{\pi K\to\kappa}(t_3, t_2, t_1) &= \sum_{\mathbf{x}_3,\mathbf{x}_1} \langle \mathrm{ReTr}[G_{t_1}(\mathbf{x}_3, t_3) G^{\dagger}_{t_2}(\mathbf{x}_3, t_3) \\ &\quad \times G^{\dagger}_{t_2}(\mathbf{x}_1, t_1)]\rangle, \\ C_{\kappa\to\pi K}(t_3, t_2, t_1) &= \sum_{\mathbf{x}_2,\mathbf{x}_1} \langle \mathrm{ReTr}[G_{t_1}(\mathbf{x}_2, t_2) G^{\dagger}_{t_3}(\mathbf{x}_2, t_2) \\ &\quad \times G^{\dagger}_{t_3}(\mathbf{x}_1, t_1)]\rangle. \end{aligned} \tag{23}$$

C. Extraction of energies

Through calculating the matrix of correlation function $C(t)$ denoted in Eq. (18), we can separate the ground state from the first excited state in a clean way. It is very important to map out ''avoided level crossings'' between the κ resonance and its decay products (namely, π and K) in a finite box volume, because the first excited state is potentially close to the ground state. This makes the extraction of the ground state energy unfeasible if we only utilize a single exponential fit ansatz. Since we cannot predict *a priori* whether our energy eigenvalues are near to the resonance region or not, we find it always safe in practice to adopt the correlation matrix to analyze our lattice simulation data for the isospin $I = 1/2$ channel. To extract the ground state, we follow the variational method [21] and construct a ratio of correlation function matrices as

$$M(t, t_R) = C(t)C^{-1}(t_R), \tag{24}$$

with some reference time slice t_R [21], which is assumed to be large enough such that the contributions to the correlation matrix $M(t, t_R)$ from the excited states can be neglected, and the lowest two eigenstates dominate the correlation function. The two lowest energy levels can be extracted by a proper fit to two eigenvalues $\lambda_n(t, t_R)$ ($n = 1, 2$) of matrix $M(t, t_R)$. Here we work on the staggered fermions, and we can easily prove that $\lambda_n(t, t_R)$ ($n = 1, 2$) behaves as [33]

$$\begin{aligned} \lambda_n(t, t_R) &= A_n \cosh\left[-E_n\left(t - \frac{T}{2}\right)\right] \\ &\quad + (-1)^t B_n \cosh\left[-E'_n\left(t - \frac{T}{2}\right)\right], \end{aligned} \tag{25}$$

for a large t, which means $0 \ll t_R < t \ll T/2$ to suppress the excited states and the unwanted contamination from ''wraparound'' effects [40–42]. This equation explicitly contains an oscillating term. For the current study, we are only interested in eigenvalue $\lambda_1(t, t_R)$; here nondegenerate eigenvalues $\lambda_1(t, t_R) > \lambda_2(t, t_R)$ are assumed. In practice, we found that the oscillating term in $\lambda_1(t, t_R)$ is not appreciable for some t_R; we can also adopt the following simple fitting model [33],

$$\lambda_1(t, t_R) = A \cosh\left[-E\left(t - \frac{T}{2}\right)\right], \tag{26}$$

and the difference between the fitting models of Eq. (25) and (26) is small. However, to make our extracted ground energy E for the isospin $I = 1/2$ channel always reliable, in this work, we will present the ground energy E calculated by Eq. (25), and then its corresponding s-wave scattering lengths.

III. LATTICE CALCULATION

A. Simulation parameters

We used the MILC lattices with $2 + 1$ dynamical flavors of the Asqtad-improved staggered dynamical fermions (the detailed description of the simulation parameters can be found in Refs. [16,17]). One thing we must stress is that the MILC configurations are generated using the staggered formulation of lattice fermions [43–45] with rooted staggered sea quarks [30] which are hypercubic-smeared [46–49]. As shown in Refs. [50,51], hypercubic-smearing gauge links significantly improves the chiral symmetry.

We analyzed πK four-point functions on the 0.15 fm MILC lattice ensemble of 450 $16^3 \times 48$ gauge

configurations with bare quark masses $am_{ud} = 0.0097$ and $am_s = 0.0484$ and bare gauge coupling $10/g^2 = 6.572$, which has a physical volume approximately 2.5 fm. The inverse lattice spacing $a^{-1} = 1.358^{+35}_{-13}$ GeV [16,17]. The mass of the dynamical strange quark is near to its physical value, and the masses of the u and d quarks are degenerate. A periodic boundary condition is applied to three spatial directions and the temporal direction.

B. Sources for isospin $I = 1/2$ channel

To calculate the πK correlation functions, we use the standard conjugate gradient method to obtain the required matrix element of the inverse fermion matrix. The calculation of the correlation function for the rectangular diagrams naturally requires us to compute the propagators on all the time slices $t_s = 0, \cdots, T-1$ of both source and sink, which requires the calculation of 48 separate propagators in our lattice simulations. After averaging the correlator over all 48 possible values, the statistics are greatly improved since we can put the pion source and kaon source at all possible time slices; namely, the correlator $C_{11}(t)$ is calculated through

$$C_{11}(t) = \langle(\pi K)(t)(\pi K)^\dagger(0)\rangle = \frac{1}{T}\sum_{t_s}\langle(\pi K)(t+t_s)(\pi K)^\dagger(t_s)\rangle. \quad (27)$$

The best effort to generate the propagators on all time slices enables us to obtain the correlators with high precision, which is vital to extract the desired scattering phase shifts reliably.

For each time slice, six fermion matrix inversions are required corresponding to the possible 3 color choices for the pion source and kaon source, respectively, and each inversion takes about 1000 iterations during the conjugate gradient calculation. Therefore, all together we carry out 288 inversions on a full QCD configuration. As shown in the following, this large number of inversions, performed on 450 configurations, provides the substantial statistics needed to resolve the real parts of the $I = 1/2$ and $3/2$ amplitudes with reliable accuracy.

In the calculation of the off-diagonal correlator, $C_{21}(t)$, the quark line contractions result in a three-point diagram since in this three-point diagram the pion field and kaon field are located at the source time slice t_s, $t_s + 1$, respectively. We calculate the off-diagonal correlator $C_{21}(t)$ through

$$C_{21}(t) = \langle\kappa(t)(\pi K)^\dagger(0)\rangle = \frac{1}{T}\sum_{t_s}\langle\kappa(t+t_s)(\pi K)^\dagger(t_s)\rangle, \quad (28)$$

where, again, we sum the correlator over all time slices t_s and average it. As for the second off-diagonal correlator $C_{12}(t)$, the pion field and kaon field are placed at the sink time slices $t_s + t$ and $t + t_s + 1$, respectively, which makes the computation of $C_{12}(t)$ difficult. However, using the relation $C_{12}(t) = C^*_{21}(t)$, we can obtain the matrix element C_{12} for free. As studied in Ref. [52], since the sink and source operators are identical for a large number of configurations, $C(t)$ is a Hermitian matrix. The $\kappa \to \pi K$ component agrees with $\pi K \to \kappa$ within the error, but the statistical errors of the matrix element C_{12} should be larger than that of matrix element C_{21} for a large t. Therefore, in the following analyses we substitute matrix element C_{12} by the complex conjugate of matrix element C_{21}, which not only saves about 20% of the computation time, but also significantly to reduces statistical errors.

For the κ correlator, $C_{22}(t)$, we have measured the point-to-point correlators with high precision in our previous work [31]. Therefore, we can exploit the available propagators to construct the κ correlator

$$C_{22}(t) = \frac{1}{T}\sum_{t_s}\langle\kappa^\dagger(t+t_s)\kappa(t_s)\rangle, \quad (29)$$

where, also, we sum the correlator over all time slices t_s and average it.

One thing we must stress is that, in the calculation of the correlator $\langle(\pi K)(\pi K)^\dagger\rangle$, we make our best effort to reliably measure the rectangular diagram, since the other two diagrams are relatively easy to evaluate. We found that the rectangular diagram plays a major role in this correlator. Therefore, we get it properly for the πK sector for the isospin $I = 1/2$ channel.

In this work, we also measure two-point correlators for the pion and kaon, namely,

$$G_\pi(t) = \langle 0|\pi^\dagger(t)\pi(0)|0\rangle, \qquad G_K(t) = \langle 0|K^\dagger(t)K(0)|0\rangle, \quad (30)$$

where the $G_\pi(t)$ is correlation function for the pion with zero momentum, and the $G_K(t)$ is correlation function for the kaon with zero momentum.

IV. SIMULATION RESULTS

In our previous work [39], we have measured the pion and kaon point-to-point correlators. Using these correlators, we can precisely extract the pion mass (m_π) and kaon mass (m_K) [39], which are summarized in Table I. Using the same method discussed in Ref. [53] and the MILC code for calculating the pion decay constants f_π, we precisely extract the pion decay constants f_π [54], which are in agreement with the previous MILC determinations at this same lattice ensemble in Ref. [17]. Here we used all the 631 lattice configurations of this ensemble. We also recapitulated these fitted values in Table I.

A. Diagrams D, C, and R

The πK four-point functions are calculated with the same lattice configurations using six u valence quarks, namely, $am_x = 0.0097$, $0.010\,67$, $0.012\,61$, $0.013\,58$,

TABLE I. Summary of the pion masses, kaon masses, and the pion decay constants. The third and fourth columns show pion masses and kaon masses in lattice units, respectively, and column five shows the pion decay constants in lattice units. The second column gives pion masses in GeV, where the errors are estimated from both the error on the lattice spacing a and the statistical errors in column three.

am_x	m_π (GeV)	am_π	am_K	af_π
0.009 70	0.334(6)	0.2459(2)	0.3962(2)	0.121 36(29)
0.010 67	0.350(6)	0.2575(2)	0.3996(2)	0.122 64(34)
0.012 61	0.379(7)	0.2789(2)	0.4066(2)	0.124 25(27)
0.013 58	0.392(7)	0.2890(2)	0.4101(2)	0.124 82(32)
0.014 55	0.406(7)	0.2987(2)	0.4134(2)	0.126 00(26)
0.019 40	0.466(8)	0.3430(2)	0.4300(2)	0.129 79(27)

0.014 55, and 0.0194, where m_x is the light valence u quark mass. They all have the same strange sea quark mass $am_s = 0.0426$, which is fixed at its physical value [17].

In Fig. 3 the individual ratios, which are defined in Eq. (15) corresponding to the diagrams in Fig. 1, R^X ($X = D$, C, and R) are displayed as the functions of t for $am_x = 0.0097$. We can note that diagram D makes the biggest contribution, then diagram C, and diagram R makes the smallest contribution. The calculation of the amplitudes for the rectangular diagram stands for our principal work. Clear signals observed up to $t = 20$ for the rectangular amplitude demonstrate that the method of the moving wall source without gauge fixing used here is practically applicable.

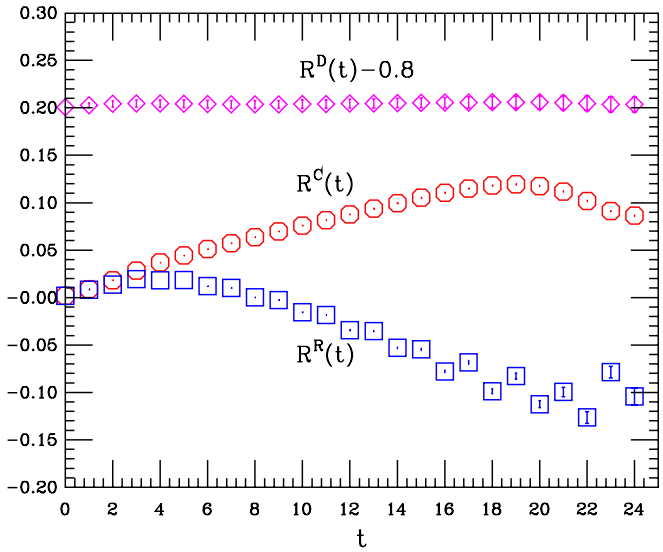

FIG. 3 (color online). Individual amplitude ratios $R^X(t)$ of the πK four-point function calculated through the moving wall source without gauge fixing as the functions of t for $am_x = 0.0097$. Direct diagram (magenta diamonds) shifted by 0.8, crossed diagram (red octagons), and rectangular diagram (blue squares).

The values of the direct amplitude R^D are quite close to unity, indicating that the interaction in this channel is very weak. The crossed amplitude, on the other hand, increases linearly, which implies a repulsion in the $I = 3/2$ channel. After an initial increase up to $t \sim 4$, the rectangular amplitude exhibits a roughly linear decrease up to $t \sim 20$, which suggests an attractive force between the pion and kaon in the $I = 1/2$ channel. Furthermore, the magnitude of the slope is similar to that of the crossed amplitude but with opposite sign. These features are what we eagerly expected from the theoretical predictions [6,24]. We can observe that the crossed and rectangular amplitudes have the same value at $t = 0$, and that there are close values for small t. Because our analytical expressions in Eq. (7) for the two amplitudes coincide at $t = 0$, they should behave similarly until the asymptotic πK state is reached.

From Fig. 3, we can clearly observe that there exists a contamination from wraparound effects [40–42] starting at $t = 18$ for the present lattice simulations of the two-meson state at finite temperature. As discussed in Ref. [13], one pion or one kaon can propagate $N_t - t$ time steps backwards which is illustrated in Fig. 6 of Ref. [13], due to the periodic boundary conditions. When the mass difference between π and K is small, this acts as a constant contribution and distorts the four-point function in the large time region [13]; luckily it is suppressed by roughly

$$\exp\left(-\frac{m_\pi + m_K}{2} N_t\right) / \exp[-(m_\pi + m_K)t]$$

compared to the forward propagation of the πK four-point function. In practice, we always select the fitting time ranges satisfying $t_{\max} \leq 16$; therefore we can reasonably neglect this contamination.

In Fig. 4, we display the ratio $R_I(t)$ projected onto the isospin $I = 1/2$ and $3/2$ channels for $am_x = 0.0097$, which are denoted in Eq. (16). A decrease of the ratio of $R_{I=3/2}(t)$ indicates a positive energy shift and hence a repulsive interaction for the $I = 3/2$ channel, while an increase of $R_{I=1/2}(t)$ suggests a negative energy shift and hence an attraction for the $I = 1/2$ channel. A dip at $t = 3$ for the $I = 1/2$ channel can be clearly observed [19]. The systematically oscillating behavior for the $I = 1/2$ channel in the large time region is also clearly observed, which is a typical characteristic of the Kogut-Susskind formulation of lattice fermions and corresponds to the contributions from the intermediate states of the opposite parity [27,28]; this also clearly indicates the existence of the contaminations from other states rather than the pion-kaon scattering state [13]. Therefore, to isolate the potential contaminations, we will use the variational method [21] to analyze the lattice simulation data. As for the $I = 3/2$ channel, this oscillating characteristic is not appreciable, and we will use the traditional method, namely, using Eq. (17) to compute the energy shift δE and then calculate the corresponding scattering length.

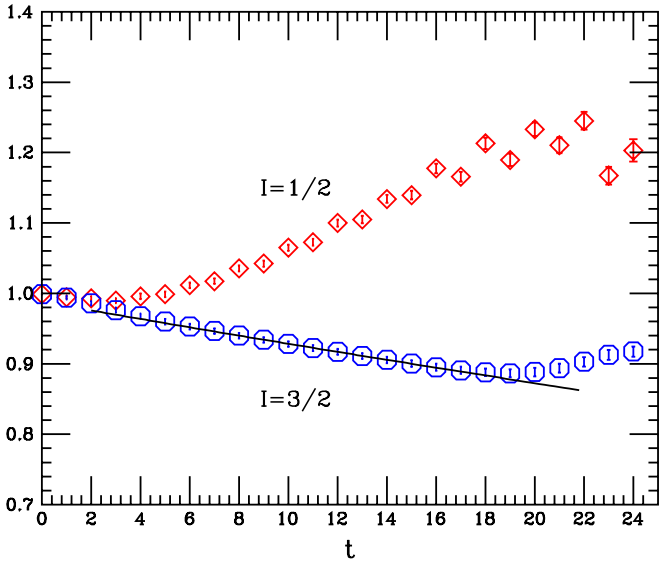

FIG. 4 (color online). $R_I(t)$ for πK four-point function at zero momenta calculated by the moving wall source without gauge fixing as the functions of t for $am_x = 0.0097$. The solid line in $I = 3/2$ is the exponential fits for $7 \leq t \leq 16$.

B. Fitting analyses for $I = 3/2$ channel

According to our discussions in Sec. II, in this work, we will make use of Eq. (17) to extract the energy shift δE for the $I = 3/2$ channel. Then we will insert these energy shifts into Eq. (9) to obtain the corresponding s-wave scattering lengths. Therefore, properly extracting the energy shifts is a crucial step to our final results in this paper. A convincing way to analyze our lattice simulation data is with the "effective energy shift" plots, a variant of the effective mass plots, where the propagators were fit with varying minimum fitting distances D_{min}, and with the maximum distance D_{max} either at 16 to suppress the contamination from wraparound effects [40–42] or where the fractional statistical errors exceeded about 20% for two successive time slices. For each valence quark m_x, the effective energy shift plots as a function of minimum fitting distance D_{min} for the $I = 3/2$ channel are shown in Fig. 5. The central value and uncertainty of each parameter were determined by the jackknife procedure over the ensemble of gauge configurations.

The energy shifts $a\delta E$ of the πK system for the $I = 3/2$ channel are extracted from the "effective energy shift" plots, and the energy shifts were selected by looking for a combination of a "plateau" in the energy as a function of the minimum distance D_{min}, and a good confidence level (namely, χ^2) for the fit. We found that the effective energy

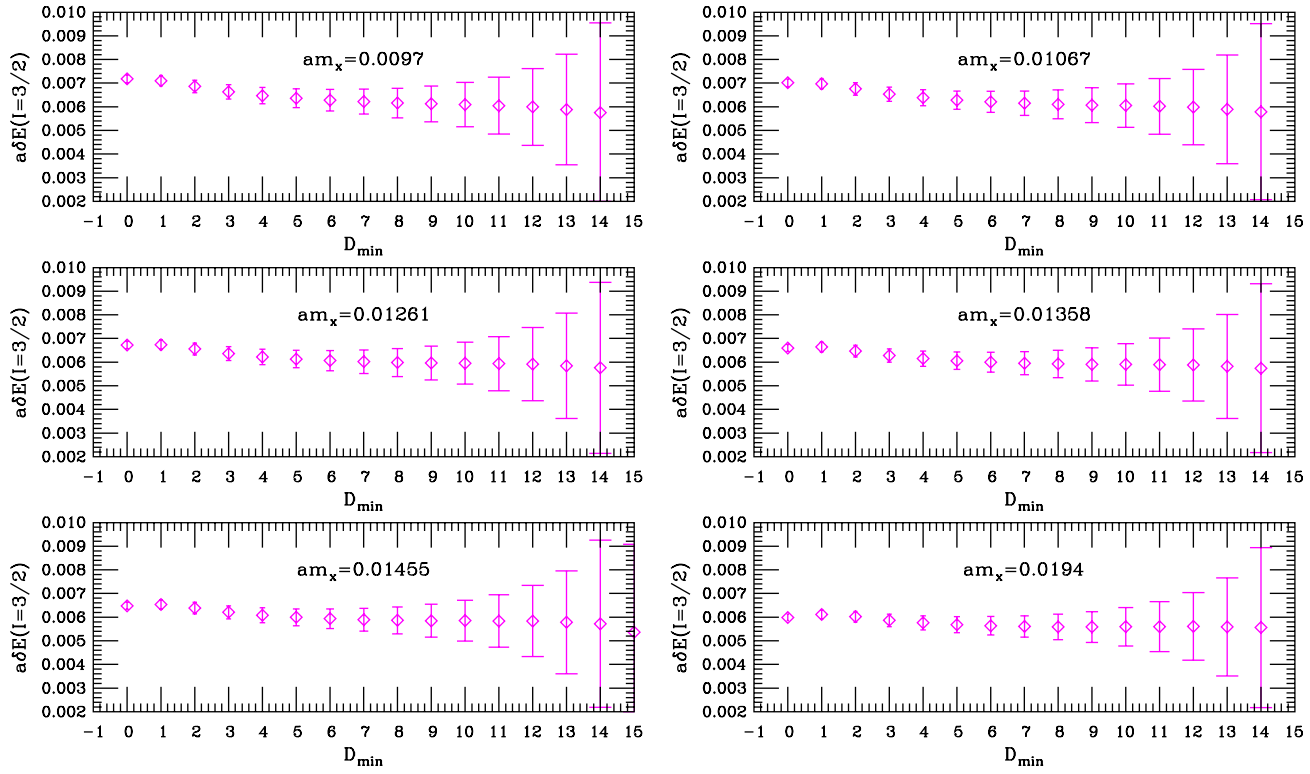

FIG. 5 (color online). The effective πK energy shift plots, $a\delta E$, as the functions of the minimum fitting distance D_{min} in the fit for the $I = 3/2$ channel. The effective πK energy shift plots for the $I = 3/2$ channel have only relatively small errors within a broad minimum distance region $5 \leq D_{\text{min}} \leq 10$.

TABLE II. Summary of the lattice simulation results for the energy shifts in lattice units for the $I = 3/2$ channel. The third column shows the energy shifts in the lattice unit, column four shows the wave function factors Z, column five shows the time range for the chosen fit, and column six shows the number of degrees of freedom (dof) for the fit. All errors are calculated from jackknife.

am_x	$a\delta E$	Z	Range	χ^2/dof
0.009 70	0.006 21(53)	0.9880(59)	7–16	0.0536/8
0.010 67	0.006 15(52)	0.9893(58)	7–16	0.0395/8
0.012 61	0.006 02(50)	0.9914(56)	7–16	0.0226/8
0.013 58	0.005 95(49)	0.9923(55)	7–16	0.0176/8
0.014 55	0.005 89(48)	0.9930(54)	7–16	0.0142/8
0.019 40	0.005 61(45)	0.9958(50)	7–16	0.0067/8

shifts for the $I = 3/2$ channel have only relatively small errors within a broad minimum time distance region $5 \leq D_{\min} \leq 10$ and are taken to be quite reliable.

We utilize the exponential physical fitting model in Eq. (17) to extract the desired energy shifts for the $I = 3/2$ channel. In Fig. 4, we display the ratio $R_I(t)$ projected onto the $I = 1/2$ and $3/2$ channels for $am_x = 0.0097$, where we can watch fitted functional form as compared with the lattice simulation data for the $I = 3/2$ channel. For the other five light u valence quarks, we obtain the similar results; therefore we do not show these ratio $R_I(t)$ plots here. The fitted values of the energy shifts, δE_I, in lattice units and wave function factor Z_I for the $I = 3/2$ channel are summarized in Table II. The wave function Z factors are pretty close to unity and the χ^2/dof is quite small for the $I = 3/2$ channel, indicating the values of the extracted scattering lengths are substantially reliable.

Now we insert the energy shifts in Table II into Eq. (9) to obtain the corresponding s-wave scattering lengths. The center-of-mass scattering momentum k^2 in GeV is calculated by Eq. (11), from which we can easily estimate its statistical errors. Once we obtain the values of k^2, the s-wave scattering lengths a_0 in lattice units can be obtained through Eq. (9). All of these values are summarized in Table III. Here we utilize pion masses and kaon masses given in Table I. The errors of the center-of-mass scattering momentum k and the s-wave scattering lengths are estimated from the statistical errors of the energy shifts energies δE, pion mass m_π, and kaon mass m_K.

C. Fitting analyses for $I = 1/2$ channel

In Fig. 6, we show the real parts of the diagonal components ($\pi K \to \pi K$ and $\kappa \to \kappa$) and the real part of the off-diagonal component $\pi K \to \kappa$ of the correlation function $C(t)$ denoted in Eq. (18). Since $C(t)$ is a Hermitian matrix, we will substitute the off-diagonal component $\kappa \to \pi K$ by $\pi K \to \kappa$ to reduce statistical errors in the following analyses.

We calculate two eigenvalues $\lambda_n(t, t_R)$ ($n = 1, 2$) for the matrix $M(t, t_R)$ in Eq. (24) with the reference time $t_R = 7$. In this work, we are only interested in the eigenvalue $\lambda_1(t, t_R)$. In Fig. 7, we plot our lattice results for $\lambda_1(t, t_R)$ for each valence quark m_x in a logarithmic scale as the functions of t together with a correlated fit to the asymptotic form given in Eq. (25) (red lines with diamonds). From these fits we then extract the energies that will be used to determine the s-wave scattering lengths.

To extract the energies reliably, we must take two major sources of the systematic errors into consideration. One arises from the excited states which affect the correlator in a low time region. The other one stems from the wrap-around effects [40–42] which distort the correlator in a high time region. By denoting a fitting range $[t_{\min}, t_{\max}]$ and varying the values of $t_{\min}$ and $t_{\max}$, we can control these

TABLE III. Summary of lattice results of the s-wave scattering lengths for the $I = 3/2$ channel. The third column shows the center-of-mass scattering momentum k^2 in GeV, column four shows the s-wave scattering lengths in lattice units, and column five shows the pion mass times scattering lengths.

am_x	k^2 [GeV^2]	a_0	$m_\pi a_0$
0.009 70	0.003 50(27)	−0.558(55)	−0.137(13)
0.010 67	0.003 57(28)	−0.569(55)	−0.146(14)
0.012 61	0.003 66(30)	−0.582(55)	−0.162(15)
0.013 58	0.003 74(30)	−0.593(56)	−0.171(16)
0.014 55	0.003 79(34)	−0.600(60)	−0.179(18)
0.019 40	0.003 96(37)	−0.624(62)	−0.214(21)

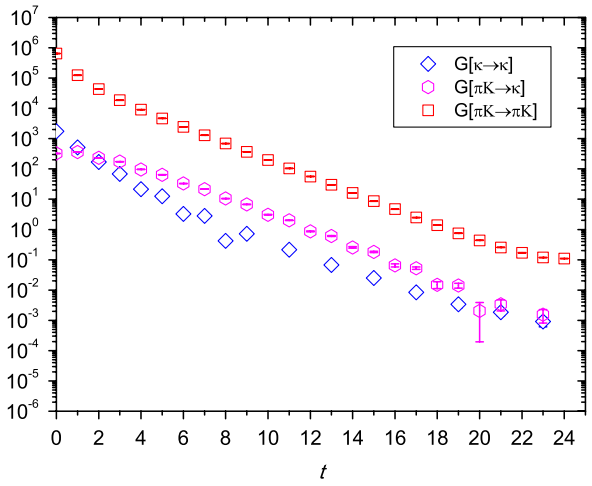

FIG. 6 (color online). Real parts of the diagonal components ($\pi K \to \pi K$ and $\kappa \to \kappa$) and the real part of the off-diagonal component $\pi K \to \kappa$ of the time correlation function $C(t)$. Occasional points with negative central values for the diagonal component $\kappa \to \kappa$ and the off-diagonal component $\pi K \to \kappa$ are not plotted.

systematic errors. In our concrete fitting, we take t_{min} to be $t_R + 1$ and increase the reference time slice t_R to suppress the excited state contaminations. Moreover, we select t_{max} to be sufficiently far away from the time slice $t = T/2$. The fitting parameters t_R, t_{min}, and t_{max} are tabulated in Table IV. The corresponding fitting results in the reasonable values of χ^2/dof. The χ^2/dof together with the fit results for the energies for the ground state aE are also listed in Table IV.

As we pointed out in Sec. II B 1, there exists a bubble contribution in the kappa correlator. To understand the effects of bubble contributions, in this work we also calculate the scattering length with the bubble contribution removed from the corresponding kappa correlator. From our discussion in Ref. [32], the time-Fourier transformation of Eq. (15) in Ref. [32] yields the bubble term $B_\kappa(t)$, which was parametrized by three low-energy couplings μ, δ_A, and δ_V. In our concrete calculation, they were fixed to the values of our previous determinations [37,39]. The taste multiplet masses in bubble terms were fixed as listed in Table VIII of Appendix B. After deducting the bubble term, the remaining kappa correlator now contains the clean information for the kappa meson; we then recalculate the eigenvalue $\lambda_1(t, t_R)$ for the matrix $M(t, t_R)$ in Eq. (24) with the reference time $t_R = 7$. In Fig. 7, we plot our lattice results for $\lambda_1(t, t_R)$ for each valence quark m_x in a logarithmic scale as the functions of t together with corresponding fitted functional forms (blue lines with octagons). Then we extract the energies which will be used to determine scattering lengths. The fitting parameters t_R, t_{min}, and t_{max} are tabulated in Table V. The corresponding fitting

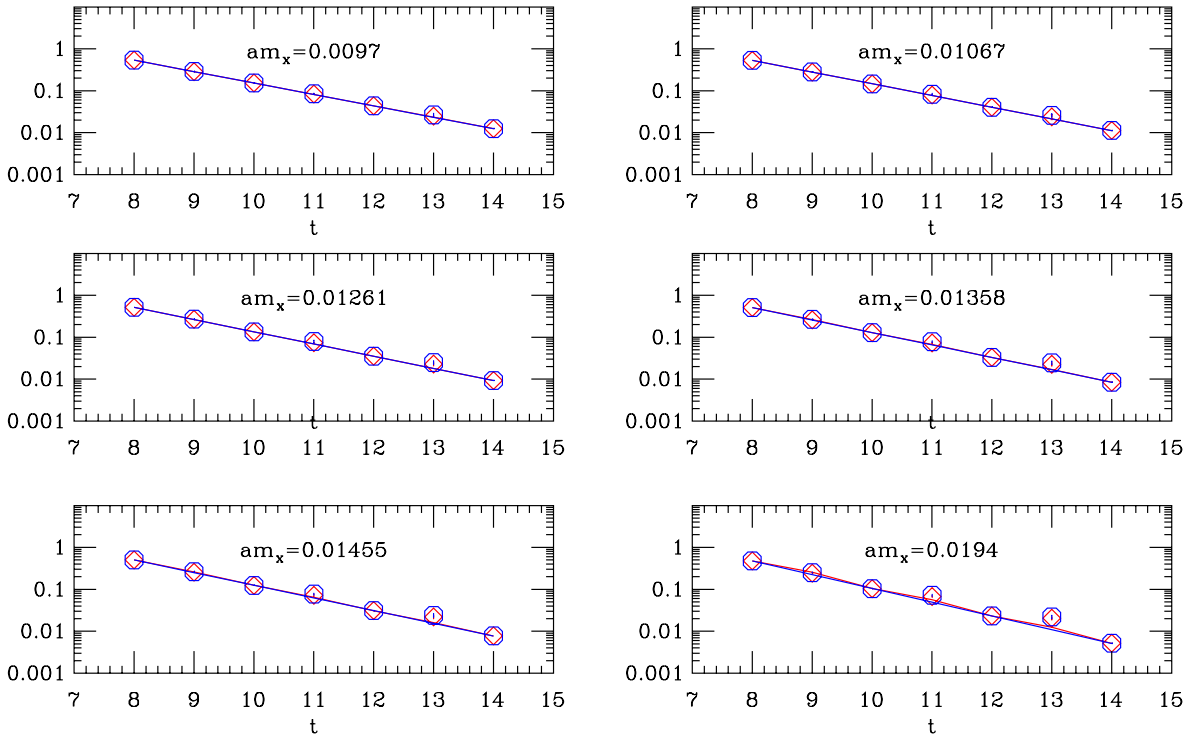

FIG. 7 (color online). The lattice results for $\lambda_1(t, t_R)$ for each valence quark m_x in a logarithmic scale as the functions of t at the $I = 1/2$ channel are shown. The solid lines are correlated fits to Eq. (25), from which the energy eigenvalues are extracted. The red lines with diamonds represent the results derived from the original kappa correlator, and the blue lines with octagons stand for the results derived from the kappa correlator with the bubble contributions deducted.

TABLE IV. Summary of the lattice simulation results for the fitted values of the energy eigenvalues for the ground state for the $I = 1/2$ channel. The third column shows the energy for the ground state in lattice units. In the table we list the reference time t_R, the lower and upper bound of the fitting range, $t_{\min}$ and $t_{\max}$, and the number of degrees of freedom (dof) for the fit quality χ^2/dof. All errors are calculated from jackknife.

am_x	aE	t_R	$t_{\min}$	$t_{\max}$	χ^2/dof
0.009 70	0.6260(6)	7	8	14	2.37/3
0.010 67	0.6412(7)	7	8	14	2.83/3
0.012 61	0.6694(10)	7	8	14	3.63/3
0.013 58	0.6828(10)	7	8	14	4.55/3
0.014 55	0.6952(11)	7	8	14	5.57/3
0.019 40	0.7561(12)	7	8	14	13.1/3

results in the reasonable values of χ^2/dof. The χ^2/dof together with the fit results for the energies for the ground state aE are also listed in Table V.

Now we insert these energies in Tables IV and V into Eq. (9) to obtain corresponding scattering lengths. The center-of-mass scattering momentum k^2 in GeV calculated by Eq. (11) and then the corresponding scattering lengths in lattice units obtained through Eq. (9) are summarized in Table VI. Here we use the pion masses and kaon masses given in Table I. The errors of the center-of-mass scattering momentum k and the scattering lengths are calculated from the statistic errors of the energy shifts energies δE, pion mass m_π, and kaon mass m_K.

From Table VI, we can clearly note that, except for $am_x = 0.0194$, the bubble terms contribute about 1%–5% differences for the final result of the scattering length. Therefore, the contamination from the bubble contribution of the kappa correlator is not large in the result of the scattering length. In the follow discussions, we will use the results including the deduction of the bubble contribution.

To examine the effects of the contaminations from the excited states for the $I = 1/2$ channel, we denote the ratios of $C_{00}(t)$ and $\mathrm{EV}[C^{-1}(t_R)C(t)]_{00}$, which is the lowest eigenvalue of $C^{-1}(t_R)C(t)$, to the πK correlator [13],

TABLE V. Summary of the lattice simulation results for the fitted values of the energy eigenvalues for the ground state for the $I = 1/2$ channel, where we subtract the bubble contribution from the kappa correlator.

am_x	aE	t_R	$t_{\min}$	$t_{\max}$	χ^2/dof
0.009 70	0.6264(4)	7	8	14	2.30/3
0.010 67	0.6414(4)	7	8	14	2.63/3
0.012 61	0.6695(7)	7	8	14	4.32/3
0.013 58	0.6828(6)	7	8	14	5.67/3
0.014 55	0.6953(5)	7	8	14	7.30/3
0.019 40	0.7547(5)	7	8	14	19.3/3

TABLE VI. Summary of the lattice simulation results of the s-wave scattering lengths for the $I = 1/2$ channel. The second column shows the center-of-mass scattering momentum k^2 in GeV, and column three shows the pion mass times scattering lengths. The fourth column shows the center-of-mass scattering momentum k^2 in GeV, where the bubble term is subtracted from the kappa correlators, and column five shows the corresponding pion mass times scattering lengths.

am_x	k^2 [GeV^2]	$m_\pi a_0$	k^2_{sub} [GeV^2]	$m_\pi a_0^{\mathrm{sub}}$
0.009 70	−0.008 84(27)	0.543(34)	−0.008 60(22)	0.522(25)
0.010 67	−0.009 04(29)	0.588(38)	−0.008 98(29)	0.582(40)
0.012 61	−0.009 56(42)	0.690(65)	−0.009 50(32)	0.685(48)
0.013 58	−0.010 10(47)	0.778(78)	−0.010 07(29)	0.775(46)
0.014 55	−0.010 75(52)	0.887(94)	−0.010 60(31)	0.868(50)
0.019 40	−0.013 43(68)	1.498(181)	−0.012 71(35)	1.355(80)

$$R_0(t) \equiv \frac{C_{00}(t)}{C_{00}(t_R)}, \qquad D_0(t) \equiv \mathrm{EV}[C^{-1}(t_R)C(t)]_{00}. \quad (31)$$

In the upper panel of Fig. 8, we show $R_0(t)$ (magenta diamonds) and $D_0(t)$ (blue octagons) at $m_\pi \simeq 0.33$ GeV. We can note that the difference of the two ratios is small. This suggests that the contamination from the excited states is negligible at this light quark mass. However, from Fig. 8(b), we observe that the contamination from

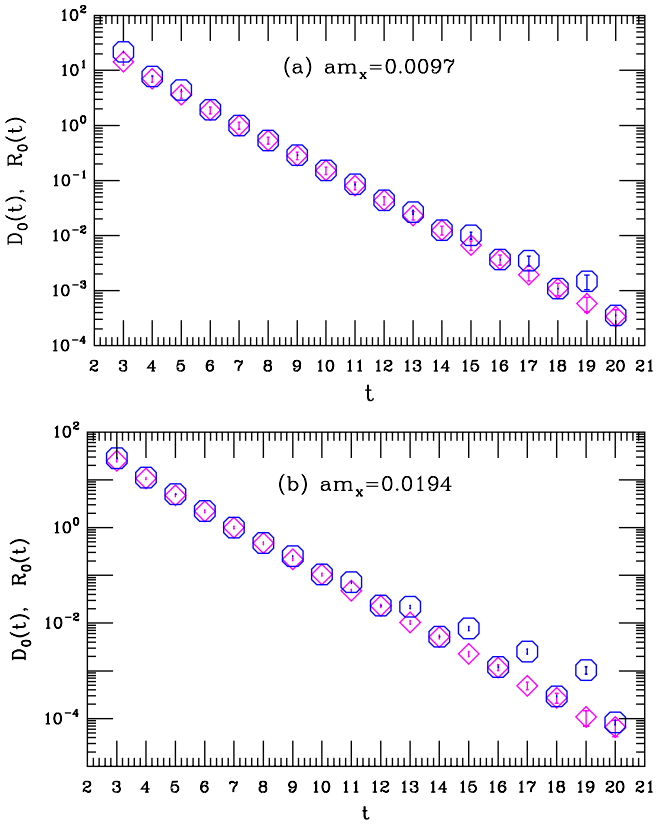

FIG. 8 (color online). $R_0(t)$ (magenta diamonds) and $D_0(t)$ (blue octagons) at (a) $am_x = 0.0097$ or $m_\pi \simeq 0.33$ GeV and (b) $am_x = 0.0194$ or $m_\pi \simeq 0.466$ GeV for the $I = 1/2$ channel.

the excited states is not negligible at $m_\pi \simeq 0.466$ GeV, and the diagonalization obviously changes the characteristics of the ratio, since the πK interpolative operator for the $I = 1/2$ channel has a large overlap with the excited states [13]. Therefore, we further confirmed that the separation of the contamination from the excited states is absolutely necessary for the heavy quark masses [13] when we study the πK scattering for the $I = 1/2$ channel.

Using the fitting models discussed in Ref. [29], we extract the pion and kaon masses [39]. And using the fitting model in Eq. (22), we calculate the kappa mass [32]. In Fig. 9, we display the m_κ, m_K, m_π, and πK threshold $m_\pi + m_K$ in lattice units as the functions of the pion mass m_π. We observe that, as the valence quark mass increases, the πK threshold grows faster than the κ mass and, as a consequence, for the heavy quark masses, the πK threshold is close to the κ mass. In Fig. 9, we can clearly note that the πK threshold is very close to the κ mass for light quark mass $am_x = 0.0194$. This can in part explain why the separation of the contamination from the excited states is indispensable for the large quark masses [13].

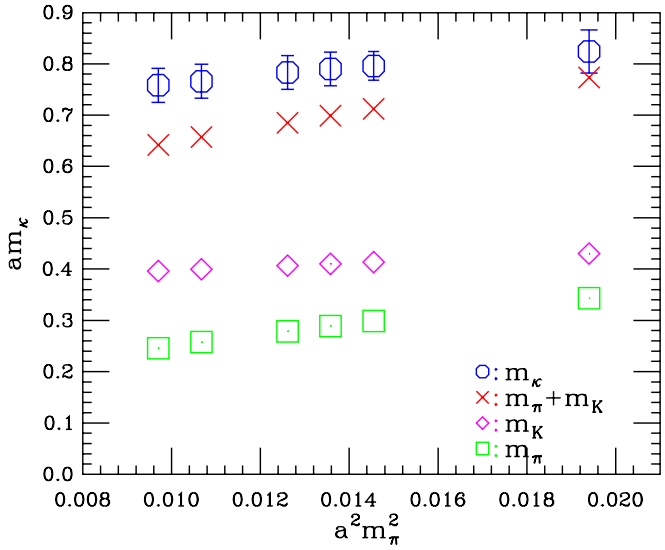

FIG. 9 (color online). Characteristics of m_κ, m_K, m_π, and $m_\pi + m_K$ in lattice units as the functions of the pion mass.

D. Chiral extrapolations and scattering length

In the present study, we employ reasonable small pion masses of m_π, namely, $m_\pi = 0.330$–0.466 GeV, which are still considerably larger than its physical ones; therefore, we need to extrapolate the s-wave πK scattering lengths toward the physical point. For this purpose, we employ the formula predicted by SU(3) chiral perturbation theory to next-to-leading order (NLO) [6,8,11,13,55]. In SU(3) chiral perturbation theory at NLO, we provide the continuum SU(3) χPT forms of $a_0^{I=(3/2)}$ and $a_0^{I=(1/2)}$, which can be directly constructed from Refs. [8,11,13],

$$
\begin{aligned}
a_0^{I=(3/2)} &= \frac{\mu_{\pi K}}{4\pi f_\pi^2}\left\{-1 + \frac{32 m_\pi m_K}{f_\pi^2} L_{\pi K}(\Lambda_\chi) - \frac{16 m_\pi^2}{f_\pi^2} L_5(\Lambda_\chi) + \frac{1}{16\pi^2 f_\pi^2}\chi_{\pi K}^{I=(3/2)}(\Lambda_\chi, m_\pi, m_K)\right\}, \\
a_0^{I=(1/2)} &= \frac{\mu_{\pi K}}{4\pi f_\pi^2}\left\{2 + \frac{32 m_\pi m_K}{f_\pi^2} L_{\pi K}(\Lambda_\chi) + \frac{32 m_\pi^2}{f_\pi^2} L_5(\Lambda_\chi) + \frac{1}{16\pi^2 f_\pi^2}\chi_{\pi K}^{I=(1/2)}(\Lambda_\chi, m_\pi, m_K)\right\},
\end{aligned}
\tag{32}
$$

where we plugged in the pion mass m_π, the kaon mass m_K, and the pion decay constant f_π, which are summarized Table I. $L_5(\Lambda_\chi)$ and $L_{\pi K}(\Lambda_\chi) \equiv 2L_1 + 2L_2 + L_3 - 2L_4 - L_5/2 + 2L_6 + L_8$ are low-energy constants defined in Ref. [56] at the chiral symmetry breaking scale Λ_χ. We should bear in mind that the expressions in Eq. (32) are written in terms of full f_π, and not its chiral limit value. The $\chi_{\pi K}^{I=(3/2)}(\Lambda_\chi, m_\pi, m_K)$ and $\chi_{\pi K}^{I=(1/2)}(\Lambda_\chi, m_\pi, m_K)$ are the known functions at NLO which clearly depend upon the chiral scale Λ_χ with chiral logarithm terms, namely,

$$
\begin{aligned}
\chi_{\pi K}^{I=(3/2)}(\Lambda_\chi, m_\pi, m_K) &= \kappa_\pi \ln\frac{m_\pi^2}{\Lambda_\chi^2} + \kappa_K \ln\frac{m_K^2}{\Lambda_\chi^2} + \kappa_\eta \ln\frac{m_\eta^2}{\Lambda_\chi^2} + \frac{86}{9} m_K m_\pi + \kappa_{\tan} \arctan\left(\frac{2(m_K - m_\pi)}{m_K + 2m_\pi}\sqrt{\frac{m_K + m_\pi}{2m_K - m_\pi}}\right), \\
\chi_{\pi K}^{I=(1/2)}(\Lambda_\chi, m_\pi, m_K) &= \kappa'_\pi \ln\frac{m_\pi^2}{\Lambda_\chi^2} + \kappa'_K \ln\frac{m_K^2}{\Lambda_\chi^2} + \kappa'_\eta \ln\frac{m_\eta^2}{\Lambda_\chi^2} + \frac{86}{9} m_K m_\pi + \frac{3}{2}\kappa_{\tan} \arctan\left(\frac{2(m_K - m_\pi)}{m_K + 2m_\pi}\sqrt{\frac{m_K + m_\pi}{2m_K - m_\pi}}\right) \\
&\quad + \kappa'_{\tan} \arctan\left(\frac{2(m_K + m_\pi)}{m_K - 2m_\pi}\sqrt{\frac{m_K - m_\pi}{2m_K + m_\pi}}\right),
\end{aligned}
\tag{33}
$$

with

$$\kappa_\pi = \frac{11m_K m_\pi^3 + 8m_\pi^2 m_K^2 - 5m_\pi^4}{2(m_K^2 - m_\pi^2)}, \qquad \kappa_K = -\frac{67m_K^3 m_\pi - 8m_\pi^3 m_K + 23m_K^2 m_\pi^2}{9(m_K^2 - m_\pi^2)},$$
$$\kappa_\eta = \frac{24m_\pi m_K^3 - 5m_K m_\pi^3 + 28m_K^2 m_\pi^2 - 9m_\pi^4}{18(m_K^2 - m_\pi^2)}, \qquad \kappa_{\tan} = -\frac{16m_K m_\pi}{9}\frac{\sqrt{2m_K^2 + m_K m_\pi - m_\pi^2}}{m_K - m_\pi},$$
$$\kappa'_\pi = \frac{11m_K m_\pi^3 - 16m_K^2 m_\pi^2 + 10m_\pi^4}{2(m_K^2 - m_\pi^2)}, \qquad \kappa'_K = -\frac{67m_K^3 m_\pi - 8m_\pi^3 m_K - 46m_K^2 m_\pi^2}{9(m_K^2 - m_\pi^2)}, \tag{34}$$
$$\kappa'_\eta = \frac{24m_\pi m_K^3 - 5m_K m_\pi^3 - 56m_K^2 m_\pi^2 + 18m_\pi^4}{18(m_K^2 - m_\pi^2)}, \qquad \kappa'_{tan} = \frac{8m_K m_\pi}{9}\frac{\sqrt{2m_K^2 - m_K m_\pi - m_\pi^2}}{m_K + m_\pi}.$$

In this work, we did not measure the η mass (m_η); instead, we utilize the Gell-Mann–Okubo mass relation to determine η mass. To improve the χPT fit, in principle, we can include all the lattice simulation data of the πK scattering lengths for both the $I = 1/2$ and $3/2$ channels to perform the simultaneous fitting. However, the fit with the data of the scattering lengths for the $I = 1/2$ channel in $m_\pi \geq 0.392$ GeV significantly increases χ^2/dof, so we only use the scattering lengths for the $I = 1/2$ channel in $m_\pi < 0.392$ GeV. The fitting results of πK scattering lengths, $m_\pi a_0^{I=3/2}$ and $m_\pi a_0^{I=1/2}$, are plotted by the dotted lines as the functions of m_π^2 in Fig. 10. The dotted lines are the chiral extrapolation of the scattering lengths for both isospin eigenstates. The fit parameters $L_{\pi K}$, L_5, and the scattering lengths $m_\pi a_0$ at the physical points (namely, $m_\pi = 0.140$ GeV, $m_K = 0.494$ GeV) [57], are also summarized in Table VII, where the chiral scale Λ_χ is taken as the physical η mass, namely, $\Lambda_\chi = 0.548$ GeV [57], as is done in Ref. [53]. The lightest (cyan) diamond points in Fig. 10 show the values of the physical scattering lengths.

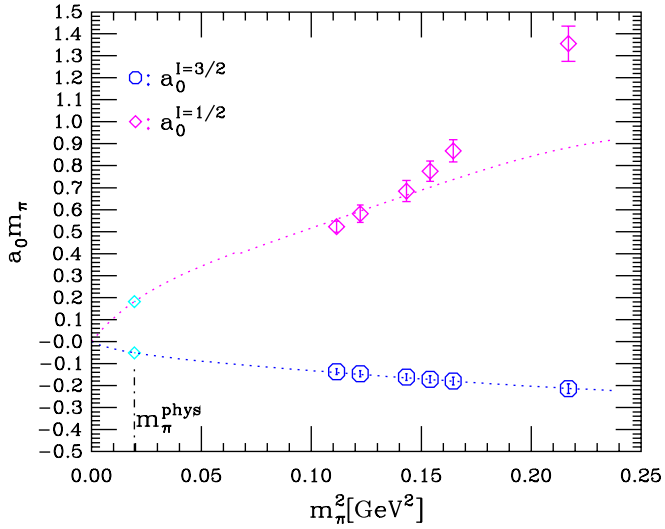

FIG. 10 (color online). m_π^2 dependence of the πK scattering lengths $m_\pi a_0$ for both the $I = 1/2$ and $3/2$ channels. The dotted lines give the SU(3) χPT predictions at NLO. The lightest (cyan) diamond points indicate its physical values.

From Fig. 10, we note that our lattice simulation results for $I = 3/2$ scattering length agree well with the one-loop formula, while scattering lengths for the $I = 1/2$ channel have a large error, and that these lattice simulation results are in reasonable agreement with the SU(3) χPT at NLO.

The fitted value of the L_5 is reasonably consistent with the value evaluated by the PACS-CS Collaboration [58], and is smaller than the corresponding result evaluated by the MILC Collaboration [53] and the NPLQCD Collaboration [11]. The fitted value of $L_{\pi K}$ is also smaller than the result evaluated by the NPLQCD Collaboration [11]. The s-wave πK scattering lengths for both the $I = 1/2$ and $3/2$ channels are in agreement with the other lattice studies [10–13].

V. SUMMARY AND OUTLOOK

In the present study, we carried out a direct lattice QCD calculation of the s-wave πK scattering lengths for both the isospin $I = 1/2$ and $3/2$ channels, where the rectangular diagram plays a crucial role, for the MILC "medium" coarse ($a = 0.15$ fm) lattice ensemble in the presence of $2 + 1$ flavors of the Asqtad-improved staggered dynamical sea quarks, generated by the MILC Collaboration. We employed the same technique in Refs. [18,19] with the moving wall sources without gauge fixing to obtain reliable precision. We calculated all the three diagrams categorized in Ref. [12], and observed a clear signal of the attraction for the $I = 1/2$ channel and that of repulsion for the $I = 3/2$ channel, respectively. Moreover, for the $I = 1/2$ channel, we employed the variational method to isolate the contamination from the excited states. We further confirmed that the separation of the contamination is absolutely necessary for the heavy quark masses [13] when we study πK scattering in the $I = 1/2$

TABLE VII. The fitted s-wave scattering lengths $m_\pi a_0$ at the physical point ($m_\pi = 0.140$ GeV, $m_K = 0.494$ GeV). The chiral scale Λ_χ is taken as the physical η mass.

χ^2/dof	$10^3 \cdot L_{\pi K}$	$10^3 \cdot L_5$	$m_\pi a_0^{I=(3/2)}$	$m_\pi a_0^{I=(1/2)}$
0.747/7	1.40(5)	1.01(12)	−0.0512(18)	0.1819(35)

channel. Simultaneously extrapolating our lattice simulation data of the s-wave scattering lengths for both isospin eigenstates to the physical point gives the scattering lengths $m_\pi a_{3/2} = -0.0512(18)$ and $m_\pi a_{1/2} = 0.1819(35)$ for the $I = 3/2$ and $1/2$ channels, respectively, which are in accordance with the current theoretical predictions to one-loop levels and the present experimental reports, and can be comparable with the other lattice studies [10–13].

A clear signal can be seen for a long time separation range in the rectangular diagram of the πK scattering. Reducing the noise by performing the calculation on a larger volume or smaller pion mass could further improve the signal to noise ratio for the rectangular diagram, and therefore obtain better results for the scattering length in the $I = 1/2$ channel [13]. Moreover, the behavior near the chiral limit is strongly affected by the chiral logarithm term; thus an evaluation without long chiral extrapolation is highly desirable to ensure the convergence of the chiral expansion [13]. Furthermore, $\tan\delta_0(k)/k$ in the low-momentum limit must be evaluated by the systematic studies with the different volumes and boundary conditions [13]. For these purposes, we are planning a series of lattice simulations on MILC coarse, fine, and superfine lattice ensembles with concentration on the lightest accessible quark masses, namely, in $m_\pi < 300$ MeV. We anticipate that these future tasks should make the calculation of the rectangular diagram more reliable.

It is well-known that πK scattering at the $I = 1/2$ channel is a more challenging and interesting channel phenomenologically due to the existence of kappa resonance. The study of the s-wave πK scattering at zero momentum is just the first step in the study of the hadron interactions including s quarks. However, it is particularly encouraging that πK scattering for the $I = 1/2$ channel can be reliably calculated by the moving wall sources without gauge fixing introduced by Kuramashi *et al.* [18,19] in spite of the essential difficulties of the calculation of the four-point functions, especially the rectangular diagram. It raises the prospect that this technique can be successfully employed to investigate the κ resonance, and so on.

In our previous work [31], we have precisely evaluated the κ mass, and found that the decay $\kappa \to \pi K$ is only allowed kinematically for small enough u quark mass. This work and our preliminary lattice simulation reported here for πK scattering lengths will encourage researchers to study the κ resonance. We are beginning a series of lattice investigations on the κ resonance parameters with isospin representation of $(I, I_z) = (1/2, 1/2)$, and the preliminary results are already reported in Refs. [33,59].

ACKNOWLEDGMENTS

This work is supported in part by Fundamental Research Funds for Central Universities under Contract No. 2010SCU23002 and the Startup Grant from the Institute of Nuclear Science and Technology of Sichuan University. The author thanks C. DeTar for kindly providing us the MILC gauge configurations used for this work and the fitting software to analyze the lattice data. We are indebted to the MILC Collaboration for using the Asqtad lattice ensemble and MILC codes. We are grateful to Hou Qing for his comprehensive support. The computations for this work were carried out at AMAX, CENTOS, and HP workstations in the Institute of Nuclear Science and Technology, Sichuan University.

APPENDIX A: THE CALCULATION METHOD OF ZETA FUNCTION

In this appendix we briefly discuss one method for numerical evaluation of zeta function $\mathcal{Z}_{00}(s; q^2)$ in the center-of-mass system for any value of q^2. Here we follow the original derivations and notations in Ref. [26].

The definition of zeta function $\mathcal{Z}_{00}(s; q^2)$ in Eq. (13) is

$$\sqrt{4\pi} \cdot \mathcal{Z}_{00}(s; q^2) = \sum_{\mathbf{n}\in\mathbb{Z}^3} \frac{1}{(n^2 - q^2)^s}. \tag{A1}$$

The zeta function $\mathcal{Z}_{00}(s; q^2)$ takes a finite value for $\mathrm{Re}\, s > 3/2$, and $\mathcal{Z}_{00}(1; q^2)$ is defined by the analytic continuation from the region $\mathrm{Re}\, s > 3/2$.

First we consider the case of $q^2 > 0$, and we separate the summation in $\mathcal{Z}_{00}(s; q^2)$ into two parts as

$$\sum_{\mathbf{n}\in\mathbb{Z}^3} \frac{1}{(n^2 - q^2)^s} = \sum_{n^2<q^2} \frac{1}{(n^2 - q^2)^s} + \sum_{n^2>q^2} \frac{1}{(n^2 - q^2)^s}. \tag{A2}$$

The second term can be written in an integral form,

$$\begin{aligned}\sum_{n^2>q^2} \frac{1}{(n^2 - q^2)^s} &= \frac{1}{\Gamma(s)} \sum_{n^2>q^2} \left[\int_0^1 dt t^{s-1} e^{-t(n^2-q^2)} + \int_1^\infty dt t^{s-1} e^{-t(n^2-q^2)} \right] \\ &= \frac{1}{\Gamma(s)} \int_0^1 dt t^{s-1} e^{q^2 t} \sum_{\mathbf{n}\in\mathbb{Z}^3} e^{-n^2 t} - \sum_{n^2<q^2} \frac{1}{(r^2 - q^2)^s} + \sum_{\mathbf{n}\in\mathbb{Z}^3} \frac{e^{-(n^2-q^2)}}{(n^2 - q^2)^s}. \end{aligned} \tag{A3}$$

The second term neatly cancels out the first term in Eq. (A2). Next we rewrite the first term in Eq. (A3) with Poisson's resummation formula as

$$\frac{1}{\Gamma(s)}\int_0^1 dt t^{s-1}e^{tq^2}\sum_{\mathbf{n}\in\mathbb{Z}^3}e^{-n^2t}=\frac{1}{\Gamma(s)}\int_0^1 dt t^{s-1}e^{tq^2}\left(\frac{\pi}{t}\right)^{3/2}\sum_{\mathbf{n}\in\mathbb{Z}^3}e^{-\pi^2n^2/t}. \quad \text{(A4)}$$

The divergence at $s=1$ comes from the $\mathbf{n}=\mathbf{0}$ part of the integrand on the right-hand side; therefore we divide the integrand into a divergent part ($\mathbf{n}=\mathbf{0}$) and a finite part ($\mathbf{n}\neq\mathbf{0}$). The divergent part can be evaluated for $\mathrm{Re}\, s>3/2$ as

$$\int_0^1 dt t^{s-1}e^{q^2t}\left(\frac{\pi}{t}\right)^{3/2}=\sum_{l=0}^{\infty}\frac{\pi^{3/2}}{s+l-3/2}\frac{q^{2l}}{l!}. \quad \text{(A5)}$$

The right-hand side of this equation takes a finite value at $s=1$.

After gathering all terms we obtain the representation of the zeta function in the center-of-mass system at $s=1$:

$$\sqrt{4\pi}\cdot Z_{00}(s;q^2)=\sum_{\mathbf{n}\in\mathbb{Z}^3}\frac{e^{-(n^2-q^2)}}{n^2-q^2}+\sum_{l=0}^{\infty}\frac{\pi^{3/2}}{l-1/2}\frac{q^{2l}}{l!}+\int_0^1 dt e^{q^2t}\left(\frac{\pi}{t}\right)^{3/2}\sum_{\mathbf{n}\in\mathbb{Z}^3}{}'e^{-\pi^2n^2/t}, \quad \text{(A6)}$$

where $\sum_{\mathbf{n}\in\mathbb{Z}^3}{}'$ stands for a summation without $\mathbf{n}=\mathbf{0}$.

For the case of $q^2\leq 0$, it is not necessary for us to separate the summation in $Z_{00}(s;q^2)$, and it can also be written in an integral form,

$$\sum_{\mathbf{n}\in\mathbb{Z}^3}\frac{1}{(n^2-q^2)^s}=\frac{1}{\Gamma(s)}\int_0^1 dt t^{s-1}e^{q^2t}\sum_{\mathbf{n}\in\mathbb{Z}^3}e^{-n^2t}+\sum_{\mathbf{n}\in\mathbb{Z}^3}\frac{e^{-(n^2-q^2)}}{(n^2-q^2)^s}. \quad \text{(A7)}$$

Following the same procedures, we arrive at the same expression in Eq. (A6). Hence, Eq. (A6) can be applied for both cases.

We also note that, for negative q^2, an exponentially convergent expression of the zeta function $Z_{00}(s;q^2)$ has been derived in Ref. [60]. We numerically compared this representation of the zeta functions with that of the above described representation, and found agreement. Therefore, we use Eq. (A6) in this work.

APPENDIX B: PSEUDOSCALAR MESON TASTE MULTIPLETS

The tree-level masses of the pseudoscalar mesons are [34,36]

$$M^2_{x,y,b}=\mu(m_x+m_y)+a^2\Delta_b, \quad \text{(B1)}$$

where x, y are two quark flavor contents which make up the meson, $b=1,\ldots,16$ are the taste, $\mu=m_\pi^2/2m_q$ is the low-energy chiral coupling constant of the point scalar current to the pseudoscalar field, and the term of $a^2\Delta_b$ comes from the taste symmetry breaking. The m_x and m_y are the two valence quark masses in the pseudoscalar meson, and m_x is the light valence u/d quark mass by convention.

We treat the u quark as a valence approximation quark, while valence strange quark mass is fixed to its physical value, so it will be convenient to introduce the notations

$$\begin{aligned}M^2_{Ub}&\equiv M_{\pi_b}=2\mu m_x+a^2\Delta_b,\\ M^2_{Sb}&\equiv M_{ss,b}=2\mu m_s+a^2\Delta_b,\\ M^2_{Kb}&\equiv M_{K_b}=\mu(m_x+m_s)+a^2\Delta_b,\end{aligned} \quad \text{(B2)}$$

where M_U is Goldstone pion mass, M_K is Goldstone kaon mass with one valence quark equal to the light valence quark and one at its physical mass, and M_S is a fictitious

TABLE VIII. The mass spectrum of the pseudoscalar meson for the MILC medium-coarse ($a=0.15$ fm) lattice ensemble with $\beta=6.572$, $am'_{ud}=0.0097$, $am'_s=0.0484$.

am_x	Taste(B)	$a\pi_B$	aK_B	$a\eta_B$	$a\eta'_B$
0.0097	P	0.2459	0.3962	0.2459	0.5018
	A	0.3724	0.4850	0.3204	0.5621
	T	0.4281	0.5289	0.4281	0.6120
	V	0.4636	0.5580	0.4484	0.6324
	I	0.4983	0.5872	0.6131	⋯
0.010 67	P	0.2575	0.3996	0.2575	0.5018
	A	0.3802	0.4878	0.3293	0.5622
	T	0.4348	0.5315	0.4348	0.6120
	V	0.4698	0.5604	0.4549	0.6325
	I	0.5042	0.5895	0.6147	⋯
0.012 61	P	0.2789	0.4066	0.2789	0.5018
	A	0.3950	0.4935	0.3460	0.5623
	T	0.4478	0.5367	0.4478	0.6120
	V	0.4819	0.5655	0.4673	0.6325
	I	0.5154	0.5943	0.6178	⋯
0.013 58	P	0.2890	0.4101	0.2890	0.5018
	A	0.4022	0.4964	0.3541	0.5624
	T	0.4542	0.5394	0.4542	0.6120
	V	0.4878	0.5680	0.4734	0.6325
	I	0.5210	0.5967	0.6193	⋯
0.014 55	P	0.2987	0.4134	0.2987	0.5018
	A	0.4092	0.4991	0.3619	0.5625
	T	0.4604	0.5419	0.4604	0.6120
	V	0.4936	0.5704	0.4793	0.6325
	I	0.5264	0.5990	0.6209	⋯
0.0194	P	0.3430	0.4300	0.3430	0.5018
	A	0.4426	0.5130	0.3986	0.5630
	T	0.4903	0.5547	0.4903	0.6120
	V	0.5216	0.5825	0.5080	0.6326
	I	0.5527	0.6105	0.6285	⋯

meson $s\bar{s}$ mass in a flavor nonsinglet state [29] with two valence quarks at physical mass.

When anomaly parameter m_0 is large, we have [31,32]

$$M^2_{\eta,I} = \tfrac{1}{3}M^2_{UI} + \tfrac{2}{3}M^2_{SI}, \qquad M_{\eta',I} = \mathcal{O}(m_0^2). \tag{B3}$$

In the taste-axial-vector sector we have

$$\begin{aligned} M^2_{\eta A} &= \frac{1}{2}\left[M^2_{UA} + M^2_{SA} + \frac{3}{4}\delta_A - Z_A\right], \\ M^2_{\eta' A} &= \frac{1}{2}\left[M^2_{UA} + M^2_{SA} + \frac{3}{4}\delta_A + Z_A\right], \\ Z^2_A &= (M^2_{SA} - M^2_{UA})^2 - \frac{\delta_A}{2}(M^2_{SA} - M^2_{UA}) + \frac{9}{16}\delta^2_A, \end{aligned} \tag{B4}$$

and likewise for $V \longrightarrow A$, where δ_V is the hairpin coupling of a pair of taste-vector mesons, and δ_A is the hairpin coupling of a pair of taste-axial mesons [53].

In the taste-pseudoscalar and taste-tensor sectors, the masses of the η_b and η'_b by definition are [31,32]

$$M^2_{\eta,b} = M^2_{Ub}; \qquad M^2_{\eta',b} = M^2_{Sb}. \tag{B5}$$

In Table VIII, we list the masses of the resulting taste multiplets in lattice units with the taste-breaking parameters δ_A and δ_V, and the mass-squared splittings $a^2\Delta_b$ determined in our previous work [39]. For the Goldstone multiplets (taste P), we measured their corresponding correlators and fitted them with a single exponential [53]. Then, using the taste splittings in Refs. [29,53], we calculated the masses of other non-Goldstone taste multiplets. We do not need the η'_I masses in this work; hence, we do not list these values in Table VIII.

[1] M. J. Matison, A. Barbaro-Galtieri, M. Alston-Garnjost, S. M. Flatté, J. H. Friedman, G. R. Lynch, M. S. Rabin, and F. T. Solmitz, Phys. Rev. D **9**, 1872 (1974).
[2] N. O. Johannesson and J. L. Petersen, Nucl. Phys. **B68**, 397 (1974).
[3] A. Karabouraris and G. Shaw, J. Phys. G **6**, 583 (1980).
[4] http://dirac.web.cern.ch/DIRAC/future.html.
[5] J. M. Flynn and J. Nieves, Phys. Rev. D **75**, 074024 (2007).
[6] V. Bernard, N. Kaiser, and U. G. Meissner, Nucl. Phys. **B357**, 129 (1991).
[7] V. Bernard, N. Kaiser, and Ulf-G. Meissner, Phys. Rev. D **43**, R2757 (1991).
[8] B. Kubis and U. G. Meissner, Phys. Lett. B **529**, 69 (2002).
[9] P. Buettiker, S. Descotes-Genon, and B. Moussallam, Eur. Phys. J. C **33**, 409 (2004).
[10] C. Miao, X. Du, G. Meng, and C. Liu, Phys. Lett. B **595**, 400 (2004).
[11] S. R. Beane, P. F. Bedaque, T. C. Luu, K. Orginos, E. Pallante, A. Parreno, and M. J. Savage, Phys. Rev. D **74**, 114503 (2006).
[12] J. Nagata, S. Muroya, and A. Nakamura, Phys. Rev. C **80**, 045203 (2009).
[13] K. Sasaki, N. Ishizuka, T. Yamazaki, and M. Oka, Prog. Theor. Phys. Suppl. **186**, 187 (2010).
[14] K. Orginos and D. Toussaint, Phys. Rev. D **59**, 014501 (1998).
[15] K. Orginos, D. Toussaint, and R. L. Sugar, Phys. Rev. D **60**, 054503 (1999).
[16] C. Bernard *et al.*, Phys. Rev. D **83**, 034503 (2011).
[17] A. Bazavov *et al.*, Rev. Mod. Phys. **82**, 1349 (2010).
[18] Y. Kuramashi, M. Fukugita, H. Mino, M. Okawa, and A. Ukawa, Phys. Rev. Lett. **71**, 2387 (1993).
[19] M. Fukugita, Y. Kuramashi, M. Okawa, H. Mino, and A. Ukawa, Phys. Rev. D **52**, 3003 (1995).
[20] M. Luscher, Nucl. Phys. **B354**, 531 (1991).
[21] M. Luscher and U. Wolff, Nucl. Phys. **B339**, 222 (1990).
[22] L. Lellouch and M. Luscher, Commun. Math. Phys. **219**, 31 (2001).
[23] M. Fukugita, Y. Kuramashi, H. Mino, M. Okawa, and A. Ukawa, Phys. Rev. Lett. **73**, 2176 (1994).
[24] S. R. Sharpe, R. Gupta, and G. W. Kilcup, Nucl. Phys. **B383**, 309 (1992).
[25] R. Gupta, G. Guralnik, G. W. Kilcup, and S. R. Sharpe, Phys. Rev. D **43**, 2003 (1991).
[26] T. Yamazaki *et al.*, Phys. Rev. D **70**, 074513 (2004).
[27] A. Mihály, H. R. Fiebig, H. Markum, and K. Rabitsch, Phys. Rev. D **55**, 3077 (1997).
[28] A. Mihály, Ph.D. thesis, Lajos Kossuth University, Debrecen, 1998.
[29] C. Aubin, C. Bernard, C. DeTar, J. Osborn, S. Gottlieb, E. B. Gregory, D. Tossaint, U. M. Heller, J. E. Hetrick, and R. Sugar, Phys. Rev. D **70**, 094505 (2004).
[30] C. Bernard, T. Burch, K. Orginos, D. Toussaint, T. A. DeGrand, C. DeTar, S. Datta, S. Gottlieb, U. M. Heller, and R. Sugar, Phys. Rev. D **64**, 054506 (2001).
[31] Z. Fu, Chinese Phys. C **35**, 1079 (2011).
[32] Z. Fu, arXiv:1111.1835 [Chin. Phys. C (to be published)].
[33] Z. Fu, J. High Energy Phys. 01 (2012) 017.
[34] C. Aubin and C. Bernard, Phys. Rev. D **68**, 034014 (2003).
[35] C. Bernard, C. E. DeTar, Z. Fu, and S. Prelovsek, Phys. Rev. D **76**, 094504 (2007).
[36] C. W. Bernard, C. E. DeTar, Z. Fu, and S. Prelovsek, Proc. Sci., LAT2006 (2006) 173.
[37] Z. W. Fu and C. DeTar, Chinese Phys. C **35**, 896 (2011).
[38] Z. Fu, Report No. UMI-32-34073.
[39] Z. W. Fu, Chin. Phys. Lett. **28**, 081 202 (2011).
[40] R. Gupta, A. Patel, and S. R. Sharpe, Phys. Rev. D **48**, 388 (1993).
[41] T. Umeda, Phys. Rev. D **75**, 094502 (2007).
[42] X. Feng, K. Jansen, and D. B. Renner, Phys. Lett. B **684**, 268 (2010).
[43] D. B. Kaplan, Phys. Lett. B **288**, 342 (1992).

[44] Y. Shamir, Nucl. Phys. **B406**, 90 (1993).
[45] Y. Shamir, Phys. Rev. D **59**, 054506 (1999).
[46] A. Hasenfratz and F. Knechtli, Phys. Rev. D **64**, 034504 (2001).
[47] T. A. DeGrand, A. Hasenfratz, and T. G. Kovacs, Phys. Rev. D **67**, 054501 (2003).
[48] T. A. DeGrand (MILC Collaboration), Phys. Rev. D **69**, 014504 (2004).
[49] S. Durr, C. Hoelbling, and U. Wenger, Phys. Rev. D **70**, 094502 (2004).
[50] D. B. Renner, W. Schroers, R. Edwards, G. T. Fleming, Ph. Hägler, J. W. Negele, K. Orginos, A. V. Pochinski, and D. Richards (LHP Collaboration), Nucl. Phys. B, Proc. Suppl. **140**, 255 (2005).
[51] R. G. Edwards, G. T. Fleming, P. Hägler, J. W. Negele, K. Orginos, A. Pochinsky, D. B. Renner, D. G. Richards, and W. Schroers (LHPC Collaboration), Proc. Sci., LAT2005 (**2006**) 056.
[52] S. Aoki *et al.* (CP-PACS Collaboration), Phys. Rev. D **76**, 094506 (2007).
[53] C. Aubin, C. Bernard, C. DeTar, J. Osborn, S. Gottlieb, E. B. Gregory, D. Toussaint, U. M. Heller, J. E. Hetrick, and R. Sugar, Phys. Rev. D **70**, 114501 (2004).
[54] Z. Fu, Commun. Theor. Phys. **57**, 78 (2012).
[55] J. W. Chen, D. O'Connell, and A. Walker-Loud, Phys. Rev. D **75**, 054501 (2007).
[56] J. Gasser and H. Leutwyler, Nucl. Phys. **B250**, 465 (1985).
[57] K. Nakamura *et al.* (Particle Data Group), J. Phys. G **37**, 075 021 (2010).
[58] S. Aoki *et al.*, Phys. Rev. D **79**, 034503 (2009).
[59] Z. Fu, Phys. Rev. D **85**, 014506 (2012).
[60] E. Elizalde, Commun. Math. Phys. **198**, 83 (1998).